Spectroscopic Screening and Binding Studies of Tripodal Amide-Thiourea Ligands as Oxoanion Receptors

Norashikin Roslan[1], Nurziana Ngah[1,2]*, Nurul Huda Abd Karim[3], Shafida Abd Hamid[1,2] and Wan Khartini Wan Abdul Khodir[1,2]

[1]Department of Chemistry, Kulliyyah of Science, International Islamic University Malaysia, Centre for Natural & Health Sciences, Jalan Sultan Ahmad Shah, 25200 Kuantan, Pahang, Malaysia

[2]Synthetic and Functional Material Research Group (SYNTOF), Department of Chemistry, Kulliyyah of Science, International Islamic University Malaysia, Centre for Natural & Health Sciences, Jalan Sultan Ahmad Shah, 25200 Kuantan, Pahang, Malaysia

[3]Department of Chemical Sciences, Faculty of Science and Technology, Universiti Kebangsaan Malaysia, 43600 Bangi, Selangor

*Corresponding author (e-mail: nurziana@iium.edu.my)

The rising levels of toxic oxoanions such as chromate, permanganate, phosphate, and arsenate in aquatic environments pose significant environmental and health concerns, necessitating the development of efficient detection systems. In this study, three tripodal amide–thiourea receptors (**AT1- AT3**) were synthesized and evaluated as supramolecular hosts for tetrahedral oxoanions. Structural characterization using UV-Vis, FTIR, and NMR spectroscopy confirmed successful formation of the receptors with multiple hydrogen-bonding donor sites. UV–Vis titration studies revealed distinct bathochromic and hypochromic spectral responses upon anion binding, indicating receptor–anion interactions via N–H·O hydrogen bonding. Job plot analysis suggested a predominant 1:1 binding stoichiometry, while binding constants (K_a) derived from BindFit ranged from 8.55×10^2 to 1.88×10^4 M^{-1}. **AT3** exhibited the highest affinity toward CrO_4^{2-}, attributed to enhanced electronic polarization and favourable structural preorganization induced by the –CN substituent. In contrast, the strongly electron-withdrawing $–NO_2$ group in **AT2** significantly decreased electron density at the thiourea binding sites through its negative inductive (–I) and negative mesomeric (–M) effects. This disrupts effective charge delocalization across the receptor framework and reduces the hydrogen bond-donating ability of the –NH moieties, ultimately resulting in weaker anion binding. These findings highlight the critical role of substituent effects in modulating anion recognition and demonstrate that tripodal amide–thiourea systems are promising candidates for selective optical sensing of environmentally relevant oxoanions.

Keywords: Amide-thiourea receptors, anion recognition, binding constant, oxoanions, supramolecular sensing, UV-Vis titration

Received: March 2026; Accepted: April 2026

Population growth, as well as agricultural and industrial activities, are major contributors to the rise of anionic pollutants in aquatic systems. These pollutants include chloride (Cl^-), nitrate (NO_3^-), chromate (CrO_4^{2-}), dichromate ($Cr_2O_7^{2-}$), permanganate (MnO_4^-), sulphate (SO_4^{2-}) and phosphate (PO_4^{3-}) [1]. Although many of these pollutants play essential roles in natural and biological systems at trace concentrations, their elevated levels in water streams can lead to serious environmental and health problems. For example, excess PO_4^{3-} contributes to eutrophication [2], NO_3^- is associated with methemoglobinemia [3], CrO_4^{2-} and $Cr_2O_7^{2-}$ are highly toxic and carcinogenic [4], Cl^- may increase water corrosivity and affect blood pressure regulation [5], while MnO_4^{2-} is a strong oxidant that can disrupt aquatic ecosystems and upon long-term exposure can cause oxidative stress, liver damage, and neurological disorders in humans [6]. Similarly, arsenate (AsO_4^{3-}), a structural analogue of phosphate, poses severe risks because of its ability to mimic phosphate in metabolic pathways, leading to carcinogenic effects, as well as cardiovascular and neurological disorders [7]. Collectively, the persistence of these anionic pollutants in aquatic environments poses significant risks to both ecosystem stability and human health.

Among these pollutants, tetrahedral oxoanions such as MnO_4^-, AsO_4^{3-}, CrO_4^{2-}, and PO_4^{3-} are particularly challenging to detect and remove. Their high hydration energy, structural symmetry, and delocalized charge distribution reduce their interactions with conventional receptors [8]. In aqueous environments, these anions are strongly solvated through hydrogen bonding (HB) with surrounding water molecules, forming stable hydration shells that must be disrupted for effective receptor binding [9].

To address these challenges, various analytical and extraction-based techniques have been developed. Conventional methods such as ion chromatography, inductively coupled plasma mass spectrometry (ICP-MS), and electrochemical methods are highly sensitive but suffer from limitations including high operational costs, complex instrumentation, and the need for skilled personnel. Recent advances have introduced alternative approaches such as switchable hydrophilicity solvent systems, supramolecular solvent-assisted microextraction for arsenic detection [10] [11], and cloud point extraction methods for MnO_4^- determination [12]. Despite their improved sensitivity, these methods often require multistep procedures and extensive sample preparation.

In contrast, optical chemosensors, particularly those based on UV-Vis spectroscopy, offer a simple, rapid, and cost-effective approach for anion detection [13]. These systems allow real-time monitoring of receptor-anion interactions through measurable spectral changes, such as bathochromic or hypsochromic shifts, as well as hyperchromicity, or hypochromicity [14]. Complementary techniques, including nuclear magnetic resonance (NMR) and infrared (IR) spectroscopy, further provide insights into binding modes and intermolecular interactions.

Supramolecular receptor design has emerged as a powerful strategy for selective anion recognition, particularly through the design of receptors with directional HB and pre-organized binding cavities which are highly suitable for the encapsulation of tetrahedral oxoanions [8, 15]. Among these, thiourea-based receptors are particularly attractive due to their strong HB donating ability arising from the –NHC=S functionality [16]. Previous studies have demonstrated their effectiveness in binding halides, carboxylates, and phosphate-containing species, highlighting their versatility [17-19]. Incorporation of amide groups into thiourea frameworks further enhances receptor performance by generating preorganized tripodal architectures with multiple convergent HB donor sites [20].

In recent years, anion recognition using thiourea-based receptors has been extensively investigated, with numerous experimental and review studies reported. For example, Manna, *et al.* demonstrated that thiourea-functionalized molecular clefts exhibited strong 1:1 binding with various oxoanions through directional HB interactions [17]. More recently, Gomez-Vega, *et al.* reported thiourea-based receptors with enhanced sensing performance toward basic anions using combined spectroscopic and computational approaches [19]. In addition, recent studies have highlighted that urea, thiourea, and squaramide motifs remain among the most effective HB donor systems for anion binding due to their dual N–H donor capability and structural tunability [21]. Furthermore, emerging work in 2025 has demonstrated that thiourea-based supramolecular receptors continue to attract significant attention for selective anion sensing, particularly in optical and fluorescence-based systems [22]. These studies collectively confirm that thiourea-based systems represent one of the most actively developed platforms in supramolecular anion recognition, with ongoing efforts focused on improving selectivity toward highly hydrated oxoanions.

Despite these advancements, achieving high selectivity and binding efficiency for strongly hydrated oxoanions remains a significant challenge. In particular, systematic investigations on how substituent electronic effects influence binding affinity and selectivity in tripodal thiourea systems are still limited. A deeper understanding of these structure–property relationships is essential for advancing the design of effective supramolecular receptors.

Therefore, this study aims to design and evaluate a series of tripodal amide–thiourea (**AT1**–**AT3**) receptors with tuneable electronic properties for selective tetrahedral oxoanion recognition. By systematically varying substituents on the thiourea moiety, this work establishes structure–property relationships governing binding affinity and selectivity. An initial screening study was conducted to assess the spectral responses of the receptors toward a range of anions, followed by detailed UV–Vis titration experiments on selected oxoanions. The binding interactions were analysed using complementary spectroscopic techniques, including Job plot analysis and binding constant determination. The results provide valuable insights into the rational design of supramolecular receptors for environmental sensing applications.

EXPERIMENTAL

Chemicals and Materials

Tris(2-aminoethyl)amine, ethyl 4-aminobenzoate, phenyl isothiocyanate, 3-nitrophenyl isothiocyanate, 3-cyanophenyl isothiocyanate, toluene, and acetonitrile were purchased from Sigma-Aldrich (USA). Sodium arsenate, potassium dichromate, potassium chromate, and potassium permanganate were obtained from Merck (Germany). All chemicals and solvents were of analytical grade and used as received without further purification.

Synthesis of AT1-AT3

Tris(2-aminoethyl)amine (1.0 mol) and ethyl 4-aminobenzoate (3.0 mol) were dissolved in toluene and refluxed under an inert atmosphere for 36 h. To the resulting reaction mixture, 3.0 mol of either phenyl isothiocyanate (**AT1**), 3-nitrophenyl isothiocyanate (**AT2**) or 3-cyanophenyl isothiocyanate (**AT3**) was added, and the mixture was stirred for an additional

24 h under the same conditions. The resulting solution was allowed to stand, and the product solidified over three days. The solid was filtered and dried to afford the products.

AT1

White solid, (89 %), m.p. 176.0-180.0 °C. ATR-FTIR (ν, cm^{-1}): 3330 (NH); 2920 (aromatic C-H); 1675 (C=O); 1240 (C-N); 1020 (C=S); 700 (C-H). UV-Vis (CH_3CN): λ_{abs} (π- π*) 221 nm, λ_{abs} (n- π*) 294 nm. ^1H NMR (500 MHz, DMSO-d_6) ppm; δ 10.12 (s, 3H, NH-2, thiourea), 10.05 (s, 3H, NH-1, thiourea), 9.62 (s, 3H, NH-3, amide), 7.92–5.95 (m, 6H, CH-4, CH-5, CH-8, CH-9, Ar-H), 4.31 (t, 7.1 Hz, 6H, CH-6, CH_2-NC=O), 4.22 (t, 7.1 Hz, 6H, CH-7, CH_2-N). ^{13}C (500MHz, DMSO-d_6) ppm: δ 166.4 (C=O, C-10), 153.9 (C=S, C-3), 131.5–113.1 (Ar-C: C-4, C-5, C-6, C-7, C-8, C-9, C-12, C-13, C-14, C-15, C-16), 59.9 (CH_2-N, C-2), 14.8 (CH_2-N, C-1). Anal. Calc. for $C_{48}H_{48}N_{10}O_3S_3$ (909.16 g/mol): C, 63.41 %; H, 5.32 %, N, 15.41 %. Found: C, 63.11 %, H, 4.97 %, N, 15.08 %.

AT2

Yellow solid, (59 %), m.p. 192.4-195.8 °C. ATR-FTIR (ν, cm^{-1}): 3320 (NH); 2925 (aromatic C-H); 1680 (C=O); 1235 (C-N); 1025 (C=S); 690 (C-H). UV-Vis (CH_3CN): λ_{abs} (π- π*) 216 nm, λ_{abs} (n- π*) 282 nm. ^1H NMR (500 MHz, DMSO-d_6) ppm; δ 10.40 (s, 3H, NH-2, thiourea), 10.02 (s, 3H, NH-1, amide), 8.56 (m, 3H, NH-3, Ar-H adjacent NO_2), 7.95 (m, 3H, CH-8, Ar-H NO_2), 7.86 (m, 6H, CH-9, Ar-H), 7.76 (m, 6H, CH-5, Ar-H), 7.71 (m, 9H, CH-4, CH-11, Ar-H), 7.59 (m, 3H, CH-10, Ar-H), 4.33 (t, J=7.1 Hz, 6H, CH-6, CH_2-NC=O), 4.21 (t, J= 7.1 Hz, 6H, CH-7, CH_2-N). ^{13}C (500 MHz, DMSO-d_6) ppm: δ 180.1 (C-10), 166.3–165.8 (C-3), 153.9 (C-13), 148.0 (C-7), 144.1 (C-4), 141.1 (C-12), 131.5–113.1 (Ar-C: C-5, C-6, C-8, C-9, C-14, C-15, C-16), 61.0–59.9 (C-2), 14.8–14.7 (C-1). Anal. Calc. for $C_{48}H_{45}N_{13}O_9S_3$ (1044.15 g/mol): C, 55.22 %; H, 4.34 %, N, 17.44 %. Found: C, 55.03 %, H, 4.2 5%, N, 17.12 %.

AT3

Pale yellow solid, (69 %), m.p. 187.0-190.0 °C. ATR-FTIR (ν, cm^{-1}): 3340 (NH); 2930 (aromatic C-H); 1670 (C=O); 1250 (C-N); 1020 (C=S); 710 (C-H). UV-Vis (CH_3CN): λ_{abs} (π- π*) 219 nm, λ_{abs} (n- π*) 287 nm. ^1H NMR (500 MHz, DMSO-d_6) ppm; δ 10.37 (s, 3H, NH-2, thiourea), 10.24 (s, 3H, NH-1, thiourea), 8.04 (s, 3H, NH-3, amide), 7.79 (m, 3H, CH-11, Ar-H CN), 7.78-7.75 (m, 9H, CH-4, CH-10), 7.76-7.71 (m, 12H, CH-5, CH-8 (m, 12H, Ar-H), 7.47 (t, J= 7.5 Hz, 3H, CH-9, Ar-H), 4.33 (t, J=7.1 Hz, 6H, CH-6, CH_2-NC=O), 4.23 (t, J=7.1 Hz, 6H, CH-7, CH_2-N). ^{13}C (500 MHz, DMSO-d_6) ppm: δ 180.1 (C-8), 166.4–165.8 (C-3), 153.8 (C-7), 144.2 (C-9), 140.7 (C-14), 131.5–111.7 (Ar-C: C-12, C-10, C-11, C-6, C-15, C-5, C-13), 61.0–59.9 (C-2), 14.8–14.7 (C-1). Anal. Calc. for $C_{51}H_{45}N_{13}O_3S_3$ (984.19 g/mol): C, 62.24 %; H, 4.61 %, N, 18.50 %. Found: C, 62.06 %, H, 4.15 %, N, 18.07 %.

Instrumentation

The melting points of the synthesized compounds were determined using an Electrothermal IA9000 series melting point apparatus. Elemental analyses (CHNS) were carried out using a 2400 Series II CHNS/O elemental analyzer (PerkinElmer). UV–Vis absorption spectra were recorded using a Shimadzu UV-1800 spectrophotometer. ATR-FTIR spectra were obtained in the range of 4000–400 cm^{-1} using a Shimadzu IRTracer-100 spectrophotometer. The ^1H and ^{13}C NMR spectra were recorded using a Bruker Avance II 400 spectrometer.

Anion Titration Studies

Stock solutions of **AT1-AT3** (1 x 10^{-5} M) were prepared in acetonitrile, while the anion solutions (1 x 10^{-3} M) were prepared in acetonitrile-deionized water (9:1, v/v). Prior to titration analysis, the anion stock solutions were diluted to 1 x 10^{-5} M. All solutions were analyzed using UV-Vis spectroscopy. Each titration was performed in triplicate to ensure reproducibility of the measurements. The UV-Vis titration data were fitted using the BindFit package v0.05, available online at https://supramolecular.org, based on a 1:1 binding model using the Nelder-Mead method.

RESULTS AND DISCUSSION

The synthesis of **AT1-AT3** involves two key stages: beginning with nucleophilic acyl substitution followed by thiourea formation. Initially, tris(2-aminoethyl) amine (TREN), which contains three primary amine groups reacts with ethyl-4-aminobenzoate under reflux in toluene. In this amidation step, the primary amine groups of TREN attack the ester carbonyl centres, generating tetrahedral intermediates that collapse to eliminate ethanol [23]. This process leads to the formation of three amide bonds, yielding a tripodal benzamide intermediate.

In the subsequent step, this intermediate reacts with the corresponding isothiocyanate. The aromatic amine group acts as a nucleophile, attacking the electrophilic carbon atom of the isothiocyanate (–N=C=S) to produce a transient zwitterionic species. This species undergoes a proton shift to afford the corresponding thiourea linkage. Each of the three arms undergoes this transformation, resulting in the tris-thiourea-substituted receptors **AT1**-**AT3** (**Figure 2**). The overall reaction mechanism is illustrated in **Figure 1**.

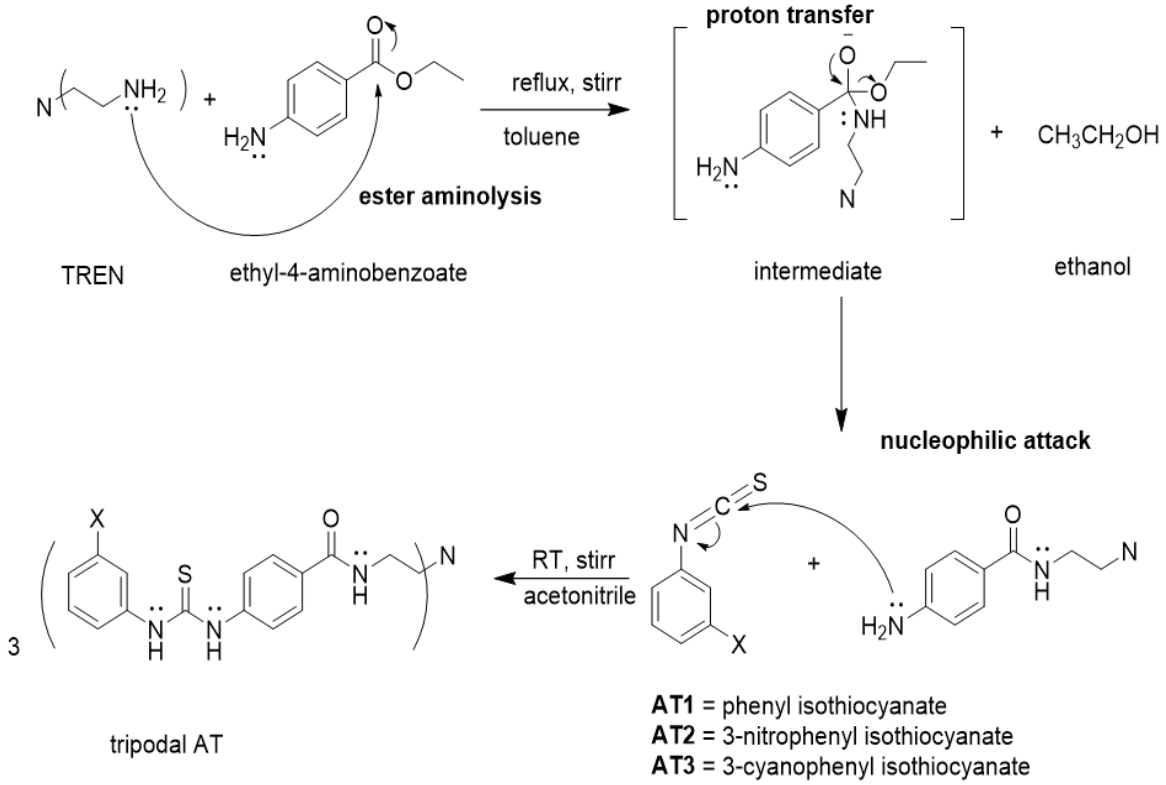

Figure 1. Mechanism for the formation of the tripodal **AT** receptors.

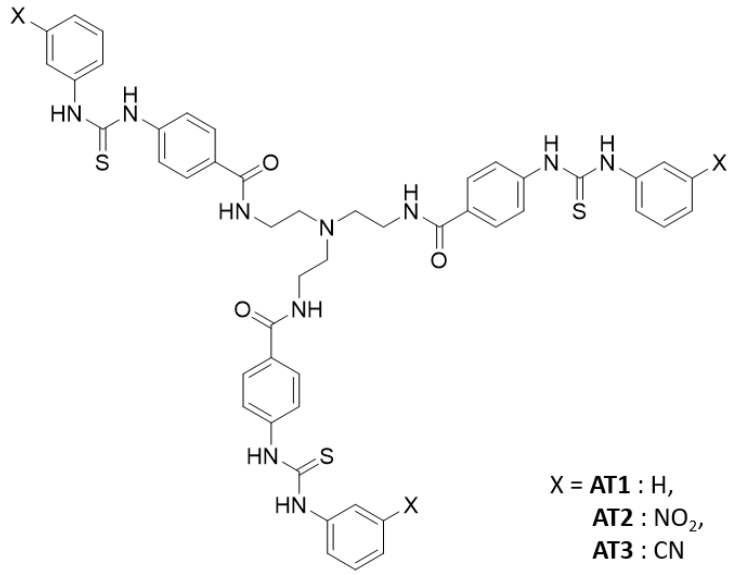

Figure 2. Chemical structure of the tripodal receptors **AT1-AT3**

FT-IR Analysis

Figure 3 shows the FT-IR spectra for **AT1-AT3,** confirming the formation of the tripodal amide-thiourea receptors and highlighting the electronic influence of the aromatic substituents. All receptors exhibited peaks characteristic of –NH stretching at 3320-3420 cm^{-1}, CH stretching at 3000-3100 cm^{-1} [24] [25], and C=O (amide) stretching at 1650-1720 cm^{-1} [26]. The thioamide (C–N) stretching vibraions were observed in the 1250-1400 cm^{-1} region [27]. The N–H peak frequencies for **AT1** and **AT3** were relatively

higher than **AT2** due to the weaker and more uniform HB interactions associated with the hydrogen and –CN substituent, which induced less perturbation of the N–H bond, and resulted in sharper, better-resolved NH stretching vibrations. In contrast, the strongly electron withdrawing $–NO_2$ in **AT2** significantly increased the N–H acidity and promoted extensive intermolecular HB interactions in the solid state, resulting in the observed band broadening and reduced sharpness [28]. Additional diagnostic peaks confirmed the presence of substituents, with **AT2** displaying the NO_2 asymmetric stretch at ~1529 cm^{-1}, while **AT3** presented the characteristic C≡N band at 2220–2260 cm^{-1}. These spectral features demonstrate that the $–NO_2$ substitution perturbed the amide–thiourea framework most significantly, while CN substitution produced moderate effects [29], while the unsubstituted **AT1** remained the least electronically perturbed.

The IR spectra also reveal that the lower transmittance (higher absorbance) values observed for **AT3** reflect stronger vibrational absorption, likely due to increased bond polarization induced by the electron-withdrawing –CN group [30]. **AT2** bears the $–NO_2$ group which promotes extensive HB networks that broaden and attenuate vibrational signals, while the –CN group enhances the dipole-moment changes for the N–H and C=O vibrations without inducing significant HB-related broadening [31]. As a result, **AT3** exhibited the highest absorption intensity, followed by **AT1** and then **AT2**.

UV-Vis Spectroscopic Studies of Tripodal AT1-AT3

The UV–Vis spectra of **AT1-AT3** (**Figure 4**) revealed two principal absorption features characteristic of amide-thiourea receptor frameworks with a high-energy π→π* band in the 200–250 nm region and a lower-energy n→π* band around 275–310 nm, consistent with documented trends for conjugated heteroatomic chromophores [32].

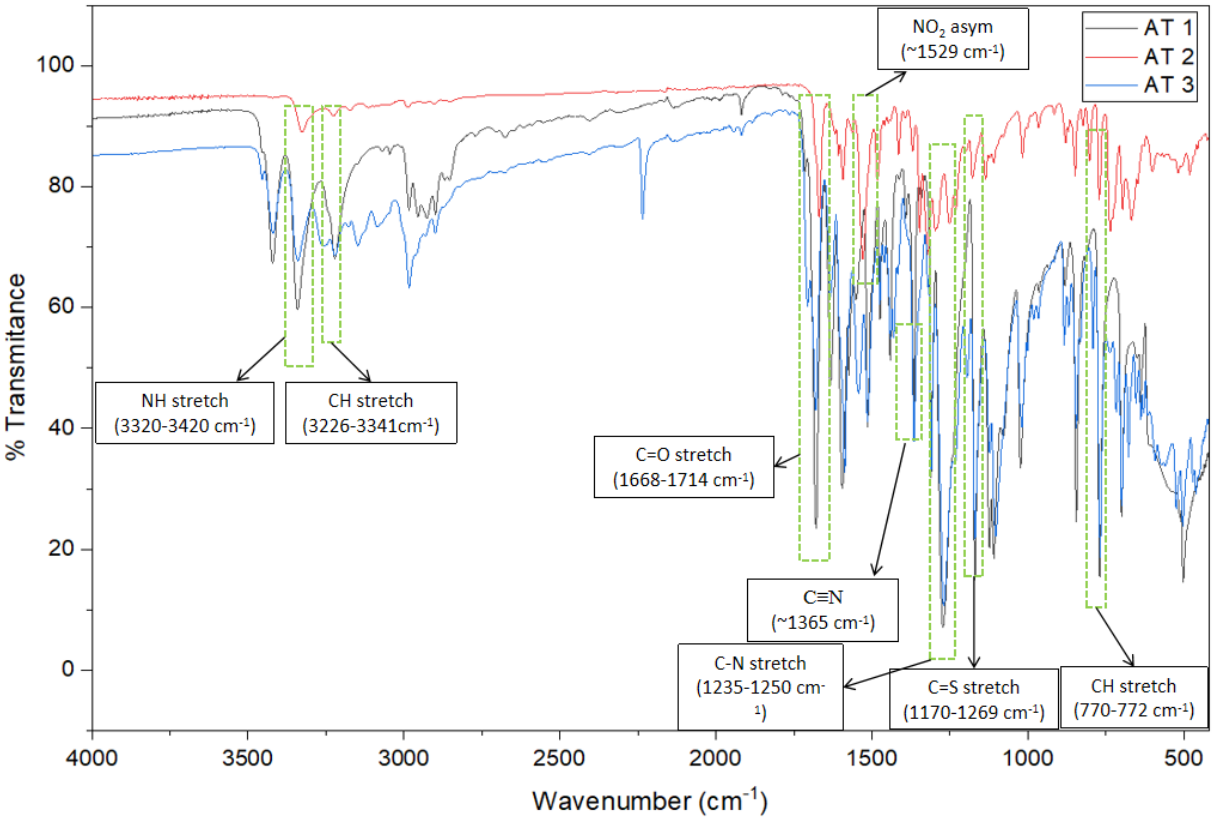

Figure 3. FTIR spectra of tripodal **AT1-AT3.**

For **AT1**, the π→π* transition was centred near ~220 nm with a relatively weak absorbance, while the n→π* band appeared at ~295 nm with a moderate intensity. The lack of strong electron-withdrawing functionality resulted in less π-electron delocalization upon excitation, and thus a lower overall absorption strength. **AT2** with *meta*-NO_2 caused a slight bathochromic shift of the π→π* band relative to **AT1**, along with a modest increase in absorption, reflecting the ability of strongly electron-withdrawing substituents to lower the energy gap between the ground and excited states by stabilizing the π framework [33]. In contrast, the n→π* transition in **AT2** had a lower intensity than in **AT3**, which may be due to intramolecular interactions such as HB between the nitro acceptor and the thiourea N–H, attenuating the nonbonding electron contribution to the transition [34]. Meanwhile, the π→π* band of **AT3** occurred at a similar wavelength to that of **AT2**, but the n→π* absorption was the most intense among the series. The cyano group, as another strong electron acceptor, enhances π-system polarization without significant intramolecular HB interference, thereby increasing the change in dipole moment associated with the n→π* transition and leading to stronger absorption [31].

Overall, these observations illustrate that meta-position electron-withdrawing substituents modulated both the positions and intensities of the electronic transitions in tripodal thiourea derivatives, with the cyano substituent producing the most pronounced enhancement of the n→π* band due to efficient polarization of the chromophore, consistent with the FTIR data.

^{1}H and ^{13}C NMR Analysis

The ^{1}H NMR spectra of receptors **AT1-AT3** were recorded in DMSO-d_6, with chemical shift assignments as shown in **Figures 5-7**. All three spectra displayed characteristic signals corresponding to thiourea and amide functionalities, aromatic rings, and alkyl linkages, confirming the successful synthesis of the designed receptors.

The ^{1}H NMR spectrum of **AT1 (Figure 5)** exhibited broad singlets at δ 10.14 and –9.82 ppm, corresponding to the NH protons of thiourea and amide groups. The nearby C=O and $CS(NH_2)_2$ groups exerted a strong deshielding effect, indicating strong HB interactions with the solvent [35]. The aromatic protons appeared as multiple overlapping signals in the range of δ 8.0–7.1 ppm, attributed to the protons on the phenyl rings. The methylene protons adjacent to the electronegative nitrogen atom and carbonyl group resonated as a multiplet at δ 4.31 and –4.22 ppm. The pronounced deshielding effect exerted by these neighbouring functional groups shifted the signal downfield from the typical aliphatic methylene region (δ 1.35–1.20 ppm) [36], thereby confirming the presence of methylene groups in the receptor framework.

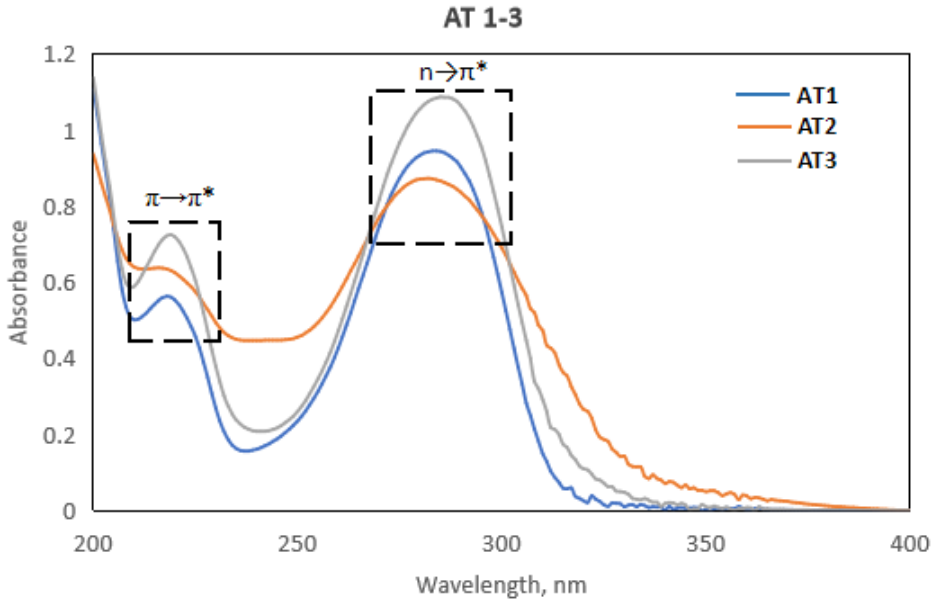

Figure 4. UV–Vis absorption spectra of **AT1**–**AT3** recorded in acetonitrile-water (9:1, v/v) (1×10^{-5} M), showing absorption bands attributed to π→π and n→π electronic transitions.

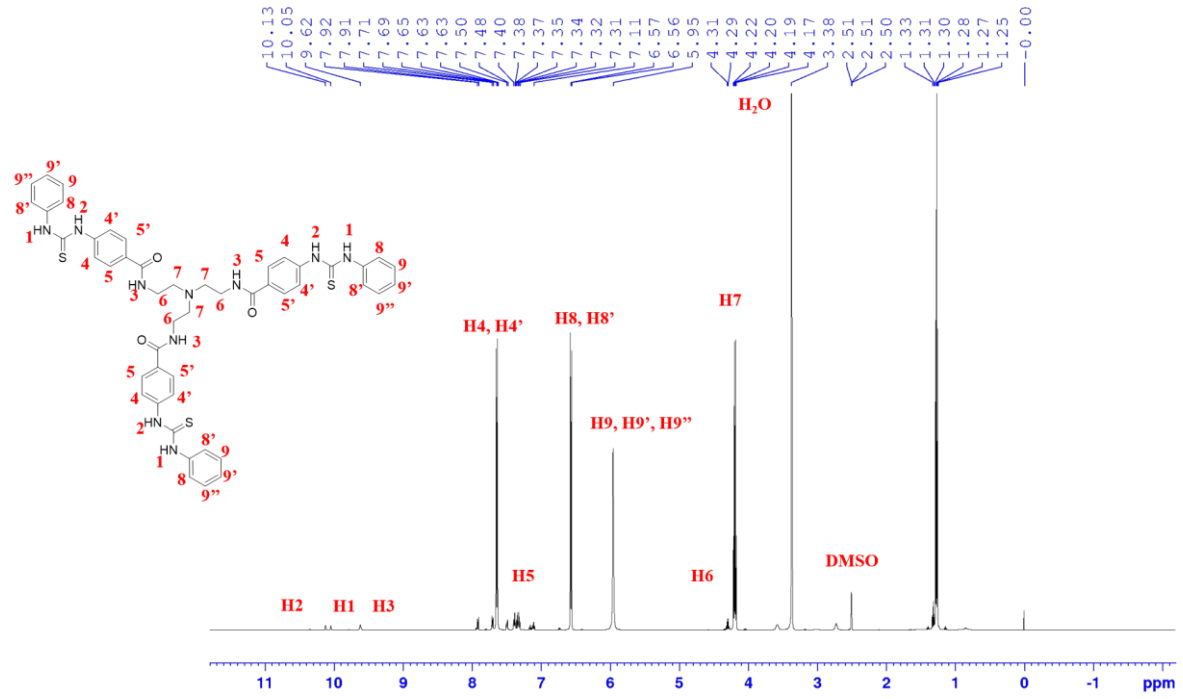

Figure 5. ^{1}H-NMR spectrum of **AT1**.

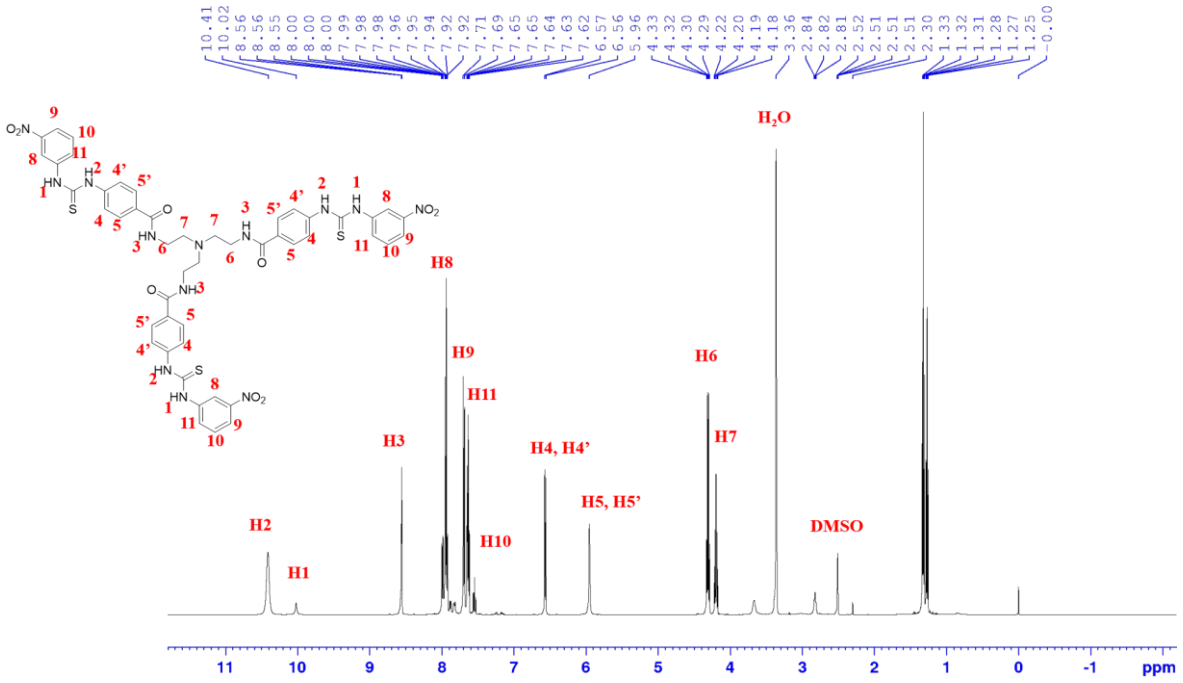

Figure 6. ^{1}H-NMR spectrum of **AT2**.

For **AT2 (Figure 6)**, the –NO_2 substituents caused a noticeable downfield shift in the spectrum. The –NH protons appeared at δ –11.22–10.40 ppm, more deshielded compared to **AT1** and **AT3**. This is attributed to the strong electron-withdrawing inductive effect of the nitro group, which reduces the electron density at the nitrogen nucleus, increasing the acidity of the NH bond and in turn enhancing its HB capability [37]. The aromatic region (δ –8.81–7.23 ppm) exhibited multiple overlapping signals and had shifted further downfield, consistent with the influence of –NO_2 substitution on the aromatic rings

[38]. As with **AT1**, **AT2** exhibited methylene resonances at δ 4.33 and –4.21 ppm, which were also shifted downfield due to the increased electron deficiency within the molecular framework [39].

The spectrum of **AT3 (Figure 7)** exhibited intermediate deshielding effects relative to **AT1** and **AT2**. The NH resonances were observed at δ –10.82–9.63 ppm, which were downfield compared to **AT1** but upfield relative to **AT2**, reflecting the moderate electron-withdrawing nature of the –CN group [40]. The aromatic signals appeared between δ –7.91 and –7.03 ppm, forming a well-defined multiplet region consistent with the symmetrical arrangement of the aromatic rings. The methylene protons observed at δ 4.33 and –4.23 ppm exhibited a similar resonance pattern to those of **AT1** and **AT2**.

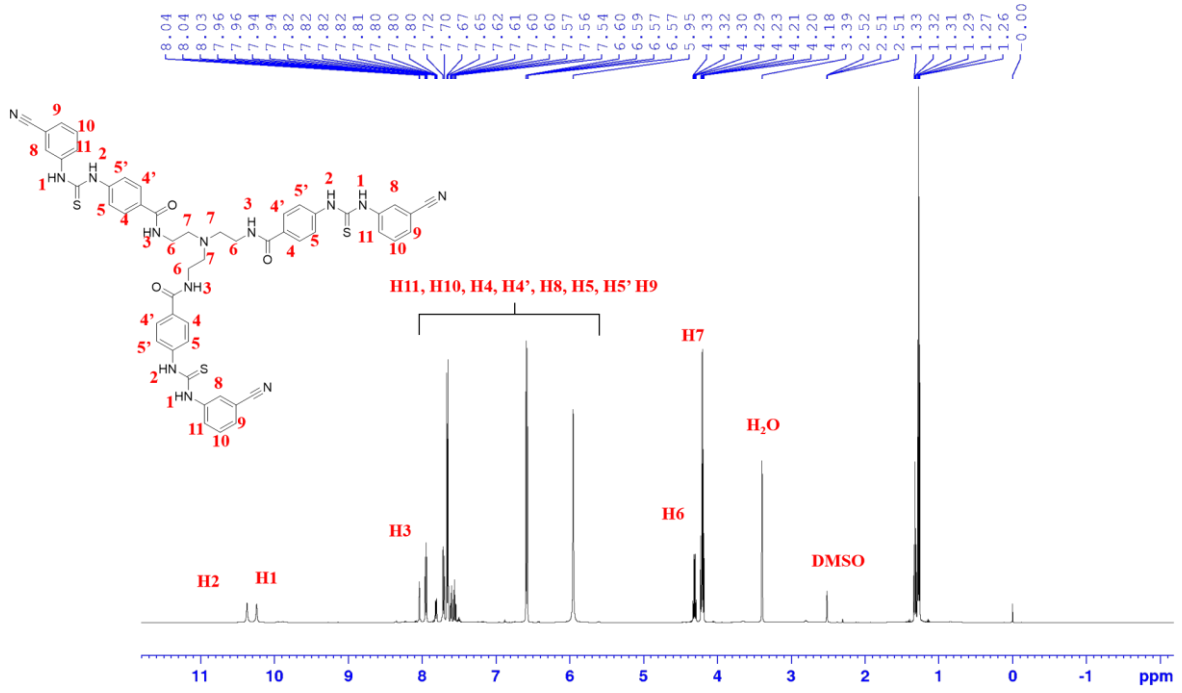

Figure 7. ^{1}H-NMR spectrum of **AT3**.

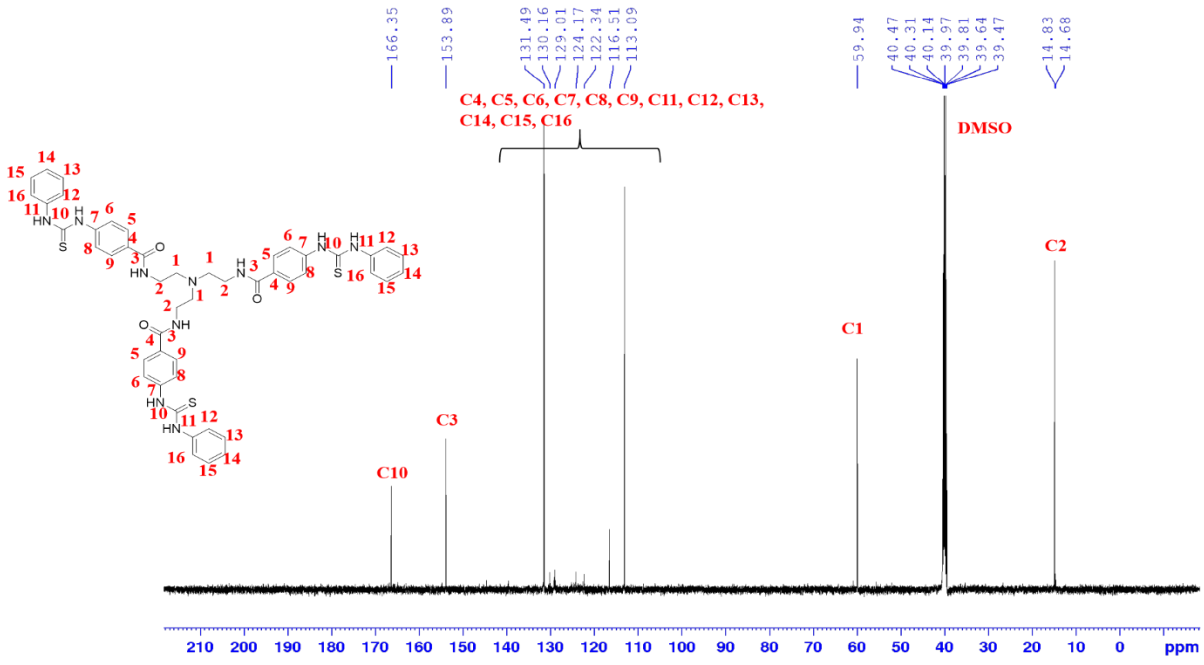

Figure 8. ^{13}C-NMR spectrum of **AT1**.

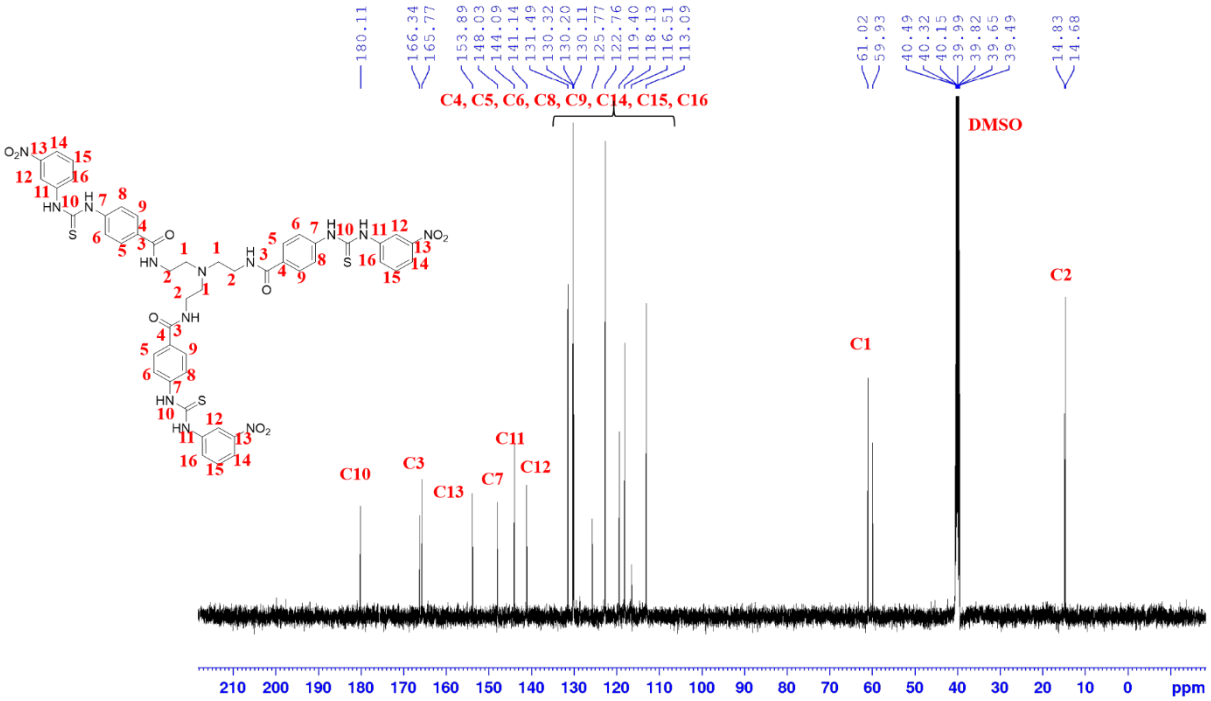

Figure 9. ^{13}C-NMR spectrum of **AT2**.

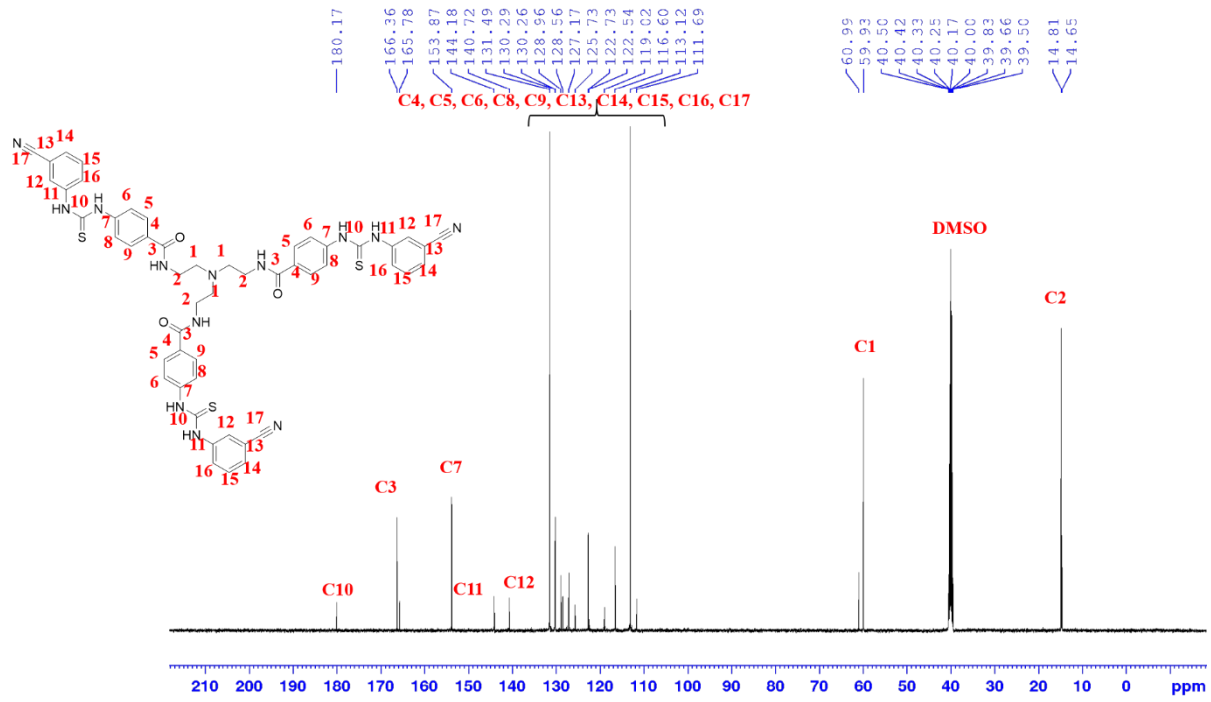

Figure 10. ^{13}C-NMR spectrum of **AT3**.

UV-Vis Studies

The binding modes of the tripodal **AT1-AT3** receptors toward various oxoanions (CrO_4^{2-}, $Cr_2O_7^{2-}$, MnO_4^-, AsO_4, CO_3^{2-}, SO_4^{2-}, and PO_4^{3-}) were investigated by UV-Vis analysis. Colorimetric analysis showed no visible colour changes upon addition of these anions (**Figure 11**, **d**). Their UV-Vis spectra, however, exhibited distinct spectral responses upon titration with the oxyanions, as shown in **Figure 11** (**a-c**). All spectra displayed two main absorption bands, corresponding to p⟶p* and n⟶p* transitions, attributed to the aromatic p-system and the –C=O and –C=S groups, respectively [32].

In all cases, the addition of anions resulted in a slight red shift (bathochromic effect) accompanied by a decrease in absorbance intensity (hypochromic effect). The bathochromic shift indicates the occurrence of HB interactions within the complexes [41]. For the free receptors, absorption bands were observed at 219 nm and 284 nm (**AT1)**, 216 nm and 282 nm (**AT2)**, and 219 nm and 287 nm (**AT3)**. Upon incremental addition of anion salts, these wavelengths shifted to 220–221 nm and 288 nm (**AT1**), 216–220 nm and 282-284 nm (**AT2**), and 219 nm and 288 nm (**AT3**).

At the lower energy band (n⟶p*), **AT1** underwent the largest red shift, followed by **AT2** and **AT3**. This phenomenon was caused by direct HB at the –C=O and –C=S regions. The electron-donating nature of **AT1** positioned the band at an energy level that was more easily stabilized upon binding. This finding is consistent with another study [42], indicating that electron-donating substituents increased orbital energy and reduced the HOMO-LUMO gap, while electron-withdrawing substituents decreased orbital energy. Meanwhile, **AT2** showed a moderate shift in this band, as the $–NO_2$ stabilized the receptor orbitals through increased –NH acidity, leading to HB formation [43]. In contrast, at the high energy (π⟶π∗) band, **AT2** exhibited the largest shift (up to 4 nm) as the $–NO_2$ group strongly withdrew electron density from the aromatic system and lowered the receptor LUMO via inductive and resonance effects [44]. Upon anion binding, this results in a greater perturbation of the aromatic π-system and its associated energy levels, suggesting a redistribution of π-electron density through polarization or charge-transfer interactions within the receptor–anion complex [45]. Furthermore, the decrease in the absorption intensity for **AT1-AT3** upon anion titration is attributed to the reduced availability of n-electrons for excitation and diminished p-electron delocalization following complex formation, leading to weakened p–p* and n–p* transitions [46].

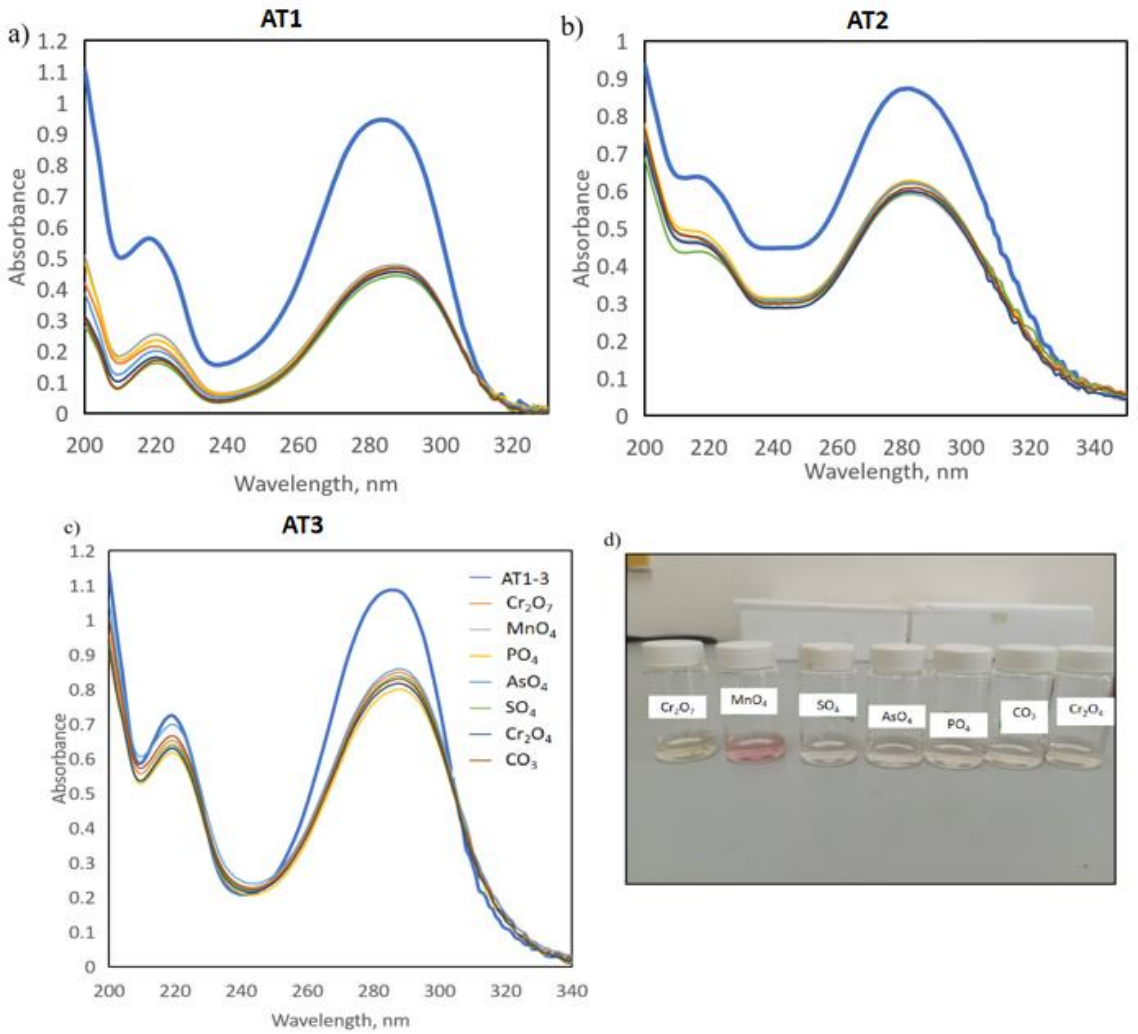

Figure 11. (a-c) UV-Vis spectra of receptors **AT1-AT3** ($1x10^{-5}$ M) upon addition of different oxoanions in MeCN/H_2O (9:1), (d) Visual appearance of **AT3** solutions in the presence of various oxoanions.

Overall, the spectral changes indicate the occurrence of receptor–anion interactions attributed to internal charge transfer (ICT) triggered by the strong interaction of oxoanions with –NH donors and the oxygen atoms of the oxyanions that perturbed the electronic environment of the chromophoric system, and led to the observed shift.

Isosbestic Point and Job Plot Analysis

In anion titration, an isosbestic point is a wavelength where the absorbance remains constant as the anion concentration increases, even though the overall spectrum changes. This behaviour indicates a direct and well-defined conversion between the free receptor and the anion-bound complex. The presence of a clear isosbestic point generally confirms the formation of a 1:1 stoichiometric complex without significant side reactions. Conversely, the absence of a clear isosbestic point suggests that the binding process is not straightforward and may involve multiple equilibria or gradual conformational changes during complex formation, multiple binding modes, deprotonation, or aggregation [47]. To further understand this binding behaviour, Job plot analysis is employed to determine the stoichiometry of the receptor–anion interaction. By systematically varying the receptor to anion ratio while keeping the total concentration constant, the maximum change in absorbance reveals the binding ratio [48]. Together, the isosbestic point analysis and Job plot provide complementary information, helping to clarify both the complexity and the stoichiometry of anion binding.

In this study, the absence of a sharp isosbestic point indicates that the binding process did not involve a simple two-species equilibrium between the free receptor and a single spectroscopically distinct complex, as displayed in **Figures 12-14.** This behaviour is common for flexible, multi-HB receptors such as tripodal amide thioureas, where anion binding induces gradual conformational rearrangements and redistribution of N–H·O interactions [49]. Consequently, the electronic transitions of the free and bound species overlap, resulting in a smooth spectral evolution rather than a fixed crossing point [50]. Despite the non-ideal isosbestic behaviour, the monotonic spectral changes clearly indicate receptor-anion interactions.

Figures **12–14** also show that the incremental addition of selected anions (AsO_4^{3-}, CrO_4^{2-}, $Cr_2O_7^{2-}$, and MnO_4^-) at 1–10 equivalents to the receptor solution resulted in a continuous decrease in absorbance. The subsequent decrease with further anion addition demonstrated electronic perturbation as the receptor-anion complex formation absorbing species decreased as the titration progresses toward saturation, resulting in a lower overall absorbance [51]. Moreover, anion binding may induce conformational changes in the tripodal receptor such as the folding of the receptor to encapsulate the anion, which alters the conjugation within the chromophore, thereby modifying its light-absorption properties. In addition, the binding of a basic anion can cause the deprotonation of acidic NH groups which also contribute to the decrease in absorbance [52].

These observations are consistent with previously reported hypochromic effects in thiourea-based and other neutral receptors during anion titration, where addition of anions induces the absorbance due to structural and electronic changes in the receptor–anion system. For instance, the intensity of the absorption spectrum of thiourea-based receptors decreased upon addition of fluoride and phosphate anions [43]. However, a further increase in the concentration of these anions resulted in no significant changes in the absorption profile. This behaviour can be attributed to the initial hydrogen bonding interaction between the anions and the acidic NH groups of the thiourea moiety, followed by deprotonation at higher anion concentrations. Once deprotonation reaches saturation, no additional receptor–anion interactions occur, leading to a plateau in the electronic perturbation of the chromophore and consequently no further observable changes in the absorption spectrum [53] [54].

Among the three receptors for **AT1** (**Figure 12**), the spectral changes observed upon anion addition were relatively small, particularly for CrO_4^{2-} and MnO_4^-. The broad and poorly defined overlap regions indicated by the arrows suggest only weak binding-induced perturbation of the electronic structure. This behaviour is consistent with **AT1** containing a phenylthiourea group as a hydrogen substituent, resulting in a comparatively low HB donor strength [55].

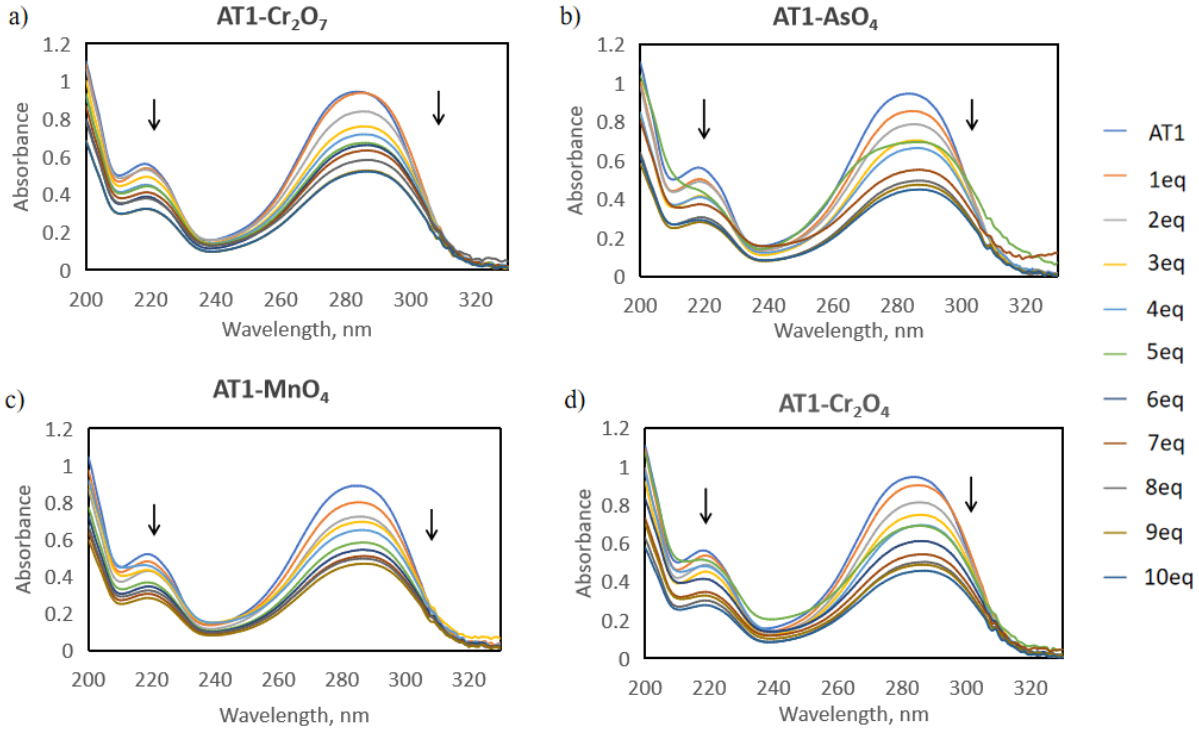

Figure 12. UV–Vis absorption spectral changes in **AT1** (1.0×10^{-5} M) upon incremental addition (0–10 equiv.) of (a) $Cr_2O_7^{2-}$, (b) AsO_4^{3-}, (c) MnO_4^-, and (d) CrO_4^{2-} in CH_3CN/H_2O (9:1, v/v) at room temperature. The arrows indicate the direction of absorbance change with increasing anion concentration.

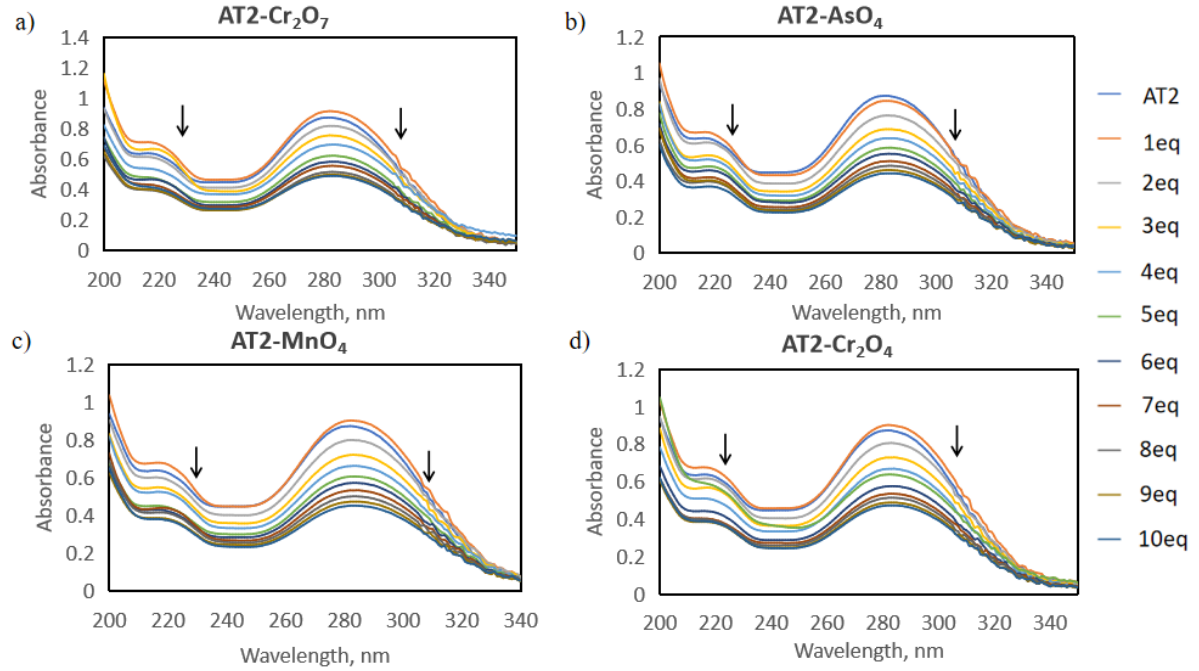

Figure 13. UV–Vis absorption spectral changes in **AT2** (1.0×10^{-5} M) upon incremental addition (0–10 equiv.) of (a) $Cr_2O_7^{2-}$, (b) AsO_4^{3-}, (c) MnO_4^-, and (d) CrO_4^{2-} in CH_3CN/H_2O (9:1, v/v) at room temperature. The arrows indicate the direction of absorbance change with increasing anion concentration.

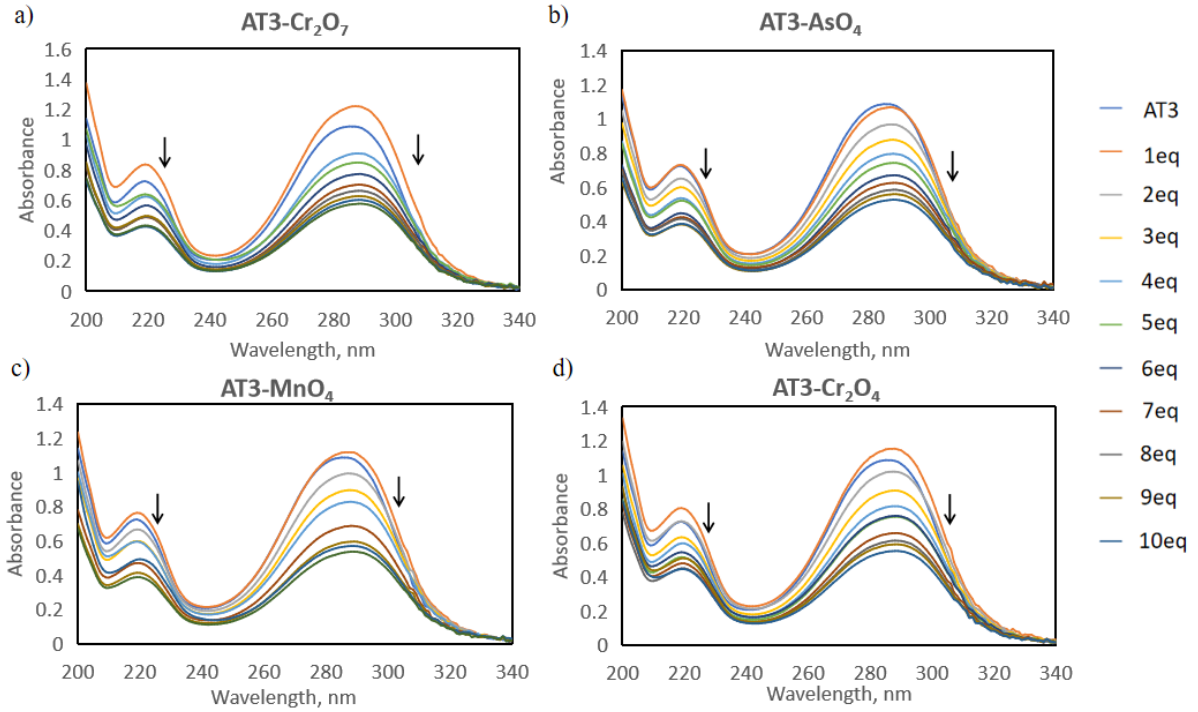

Figure 14. UV–Vis absorption spectral changes in **AT3** (1.0×10^{-5} M) upon incremental addition (0–10 equiv.) of (a) $Cr_2O_7^{2-}$, (b) AsO_4^{3-}, (c) MnO_4^-, and (d) CrO_4^{2-} in CH_3CN/H_2O (9:1, v/v) at room temperature. The arrows indicate the direction of absorbance change with increasing anion concentration.

In contrast, **AT2** (**Figure 13**) displayed more noticeable and systematic spectral changes for all four anions. Although a distinct isosbestic point was not observed, the spectra evolved more regularly, with a clearer reduction in the original absorption bands. Despite the presence of an electron-withdrawing substituent, the meta substitution in **AT2** limited effective resonance communication with the thiourea moiety, resulting in only moderate NH polarisation and comparatively weaker anion binding strength. Nevertheless, the strong inductive electron-withdrawing nature of the $–NO_2$ group increased the acidity of the thiourea NH protons, thereby promoting more uniform receptor–anion hydrogen bonding interactions and stabilising the resulting complexes [18].

The spectral responses were even more pronounced in **AT3** (**Figure 14**), reflecting a more effective transmission of electron-withdrawing influence toward the thiourea moiety. Although the –CN substituent is intrinsically weaker than $–NO_2$, its electronic effect was more efficiently relayed within the molecular framework of **AT3**, leading to enhanced thiourea NH acidity and amplified binding-induced electronic perturbation. Consequently, there was stronger HB donation to oxoanion groups, resulting in a more significant redistribution of electron density within the conjugated system and a substantial decrease in absorbance intensity, particularly in the 270–290 nm region [56].

Although a well-defined isosbestic point was not observed throughout this UV–Vis titration, likely due to the presence of multiple equilibria involving hydrogen bonding interactions and partial deprotonation of the thiourea NH groups, the Job plot analysis suggests that a 1:1 receptor–anion interaction was the predominant binding mode [57]. The Job plots (**Figure 15**–**17**) exhibited symmetrical parabolic profiles with maxima centred at a molar fraction of approximately $X_R = 0.5$ for all oxoanions investigated (AsO_4^{3-}, CrO_4^{2-}, $Cr_2O_7^{2-}$, and MnO_4^-). The tripodal receptors **AT1**–**AT3** possess a preorganized cavity comprising three flexible arms bearing HB donor (thiourea –NH) and acceptor (amide –NH and –C=O) sites capable of forming multiple N–H·O interactions with tetrahedral oxoanions. Thus, the dominant spectroscopically responsive species is consistent with a 1:1 receptor–anion complex.

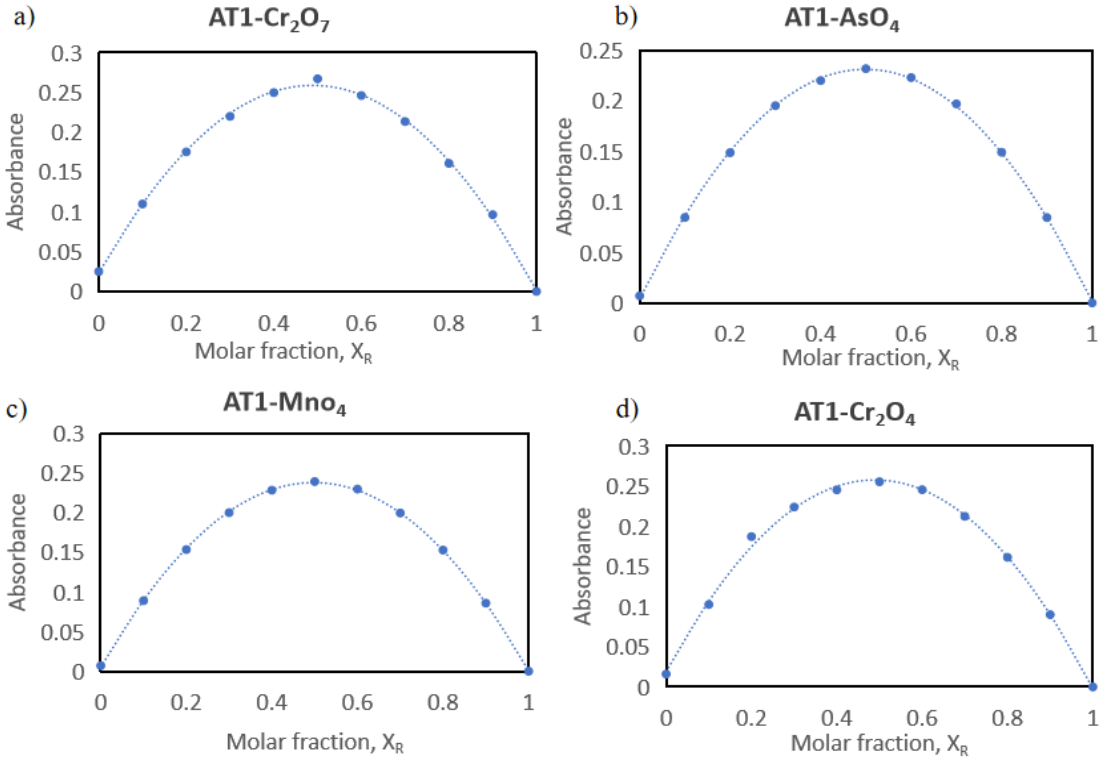

Figure 15. Job's plots of **AT1** with (a) $Cr_2O_7^{2-}$, (b) AsO_4^{3-}, (c) MnO_4^{-}, and (d) CrO_4^{2-} based on UV–Vis measurements in acetonitrile–deionized water (9:1, v/v). The maximum absorbance at $X_R \approx 0.5$ indicates a 1:1 binding stoichiometry between **AT1** and the respective anions.

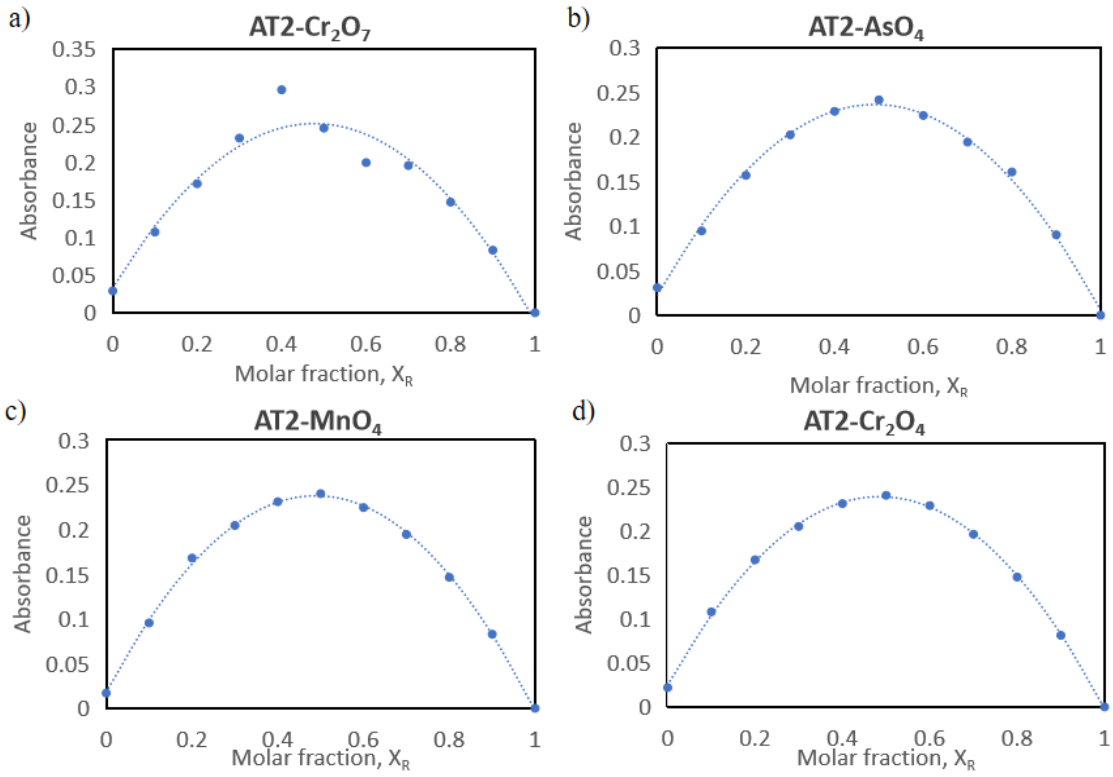

Figure 16. Job's plots of **AT2** with (a) $Cr_2O_7^{2-}$, (b) AsO_4^{3-}, (c) MnO_4^{-}, and (d) CrO_4^{2-} based on UV–Vis measurements in acetonitrile–deionized water (9:1, v/v). The maximum absorbance at $X_R \approx 0.5$ indicates a 1:1 binding stoichiometry between **AT2** and the respective anions.

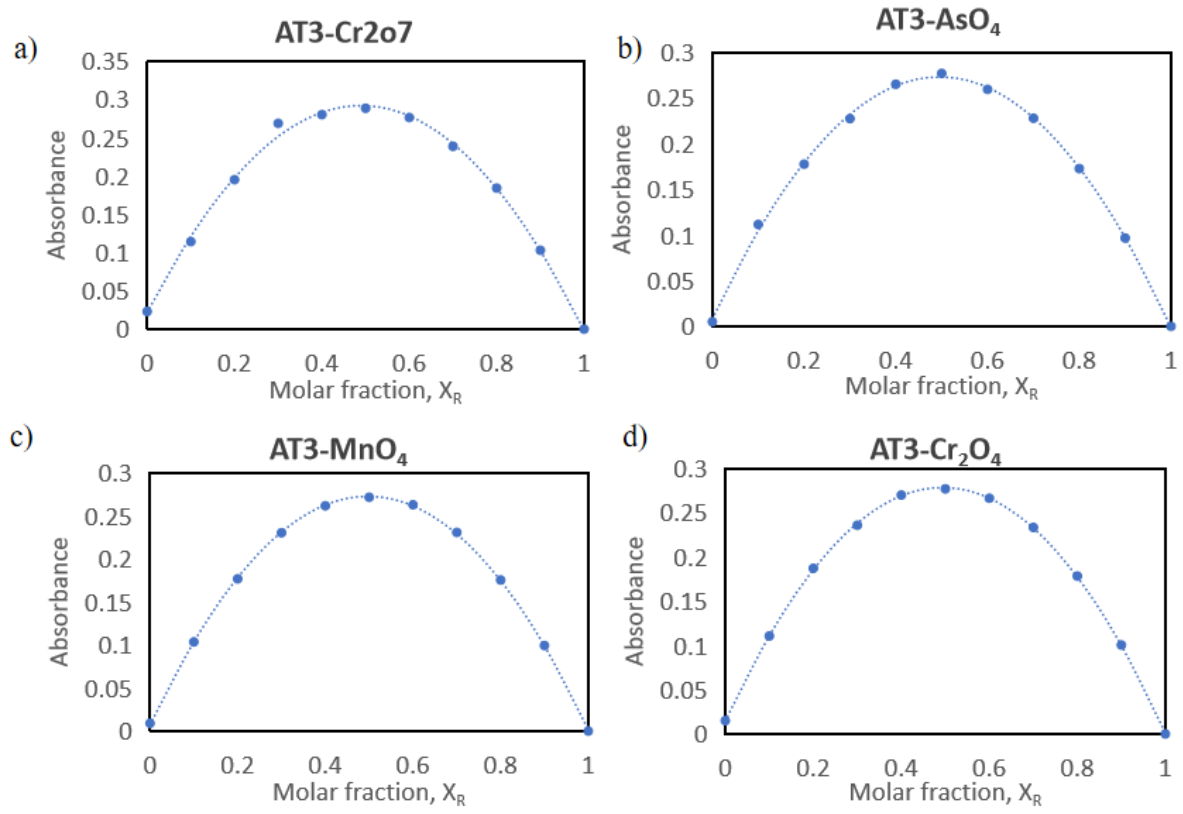

Figure 17. Job's plots of **AT3** with (a) $Cr_2O_7^{2-}$, (b) AsO_4^{3-}, (c) MnO_4^{-}, and (d) CrO_4^{2-} based on UV–Vis measurements in acetonitrile–deionized water (9:1, v/v). The maximum absorbance at $X_R \approx 0.5$ indicates a 1:1 binding stoichiometry between **AT3** and the respective anions.

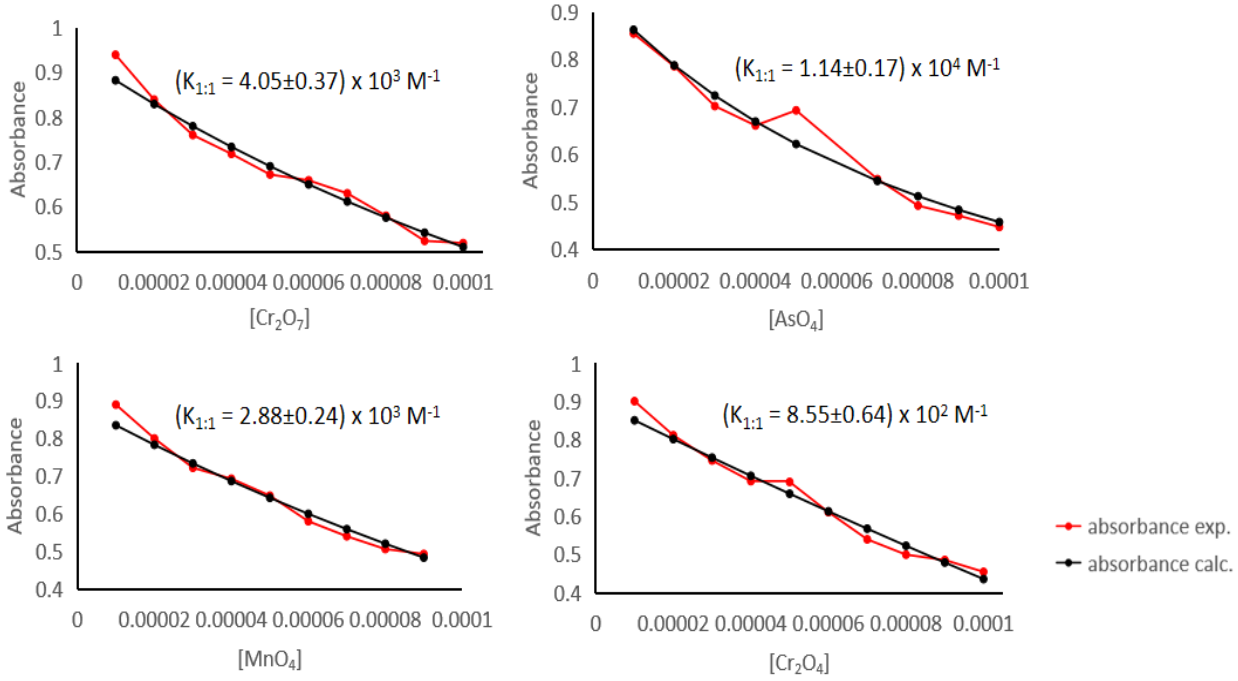

Figure 18. UV–Vis titration plots of **AT1** with $Cr_2O_7^{2-}$, AsO_4^{3-}, MnO_4^{-}, and CrO_4^{2-} showing experimental and calculated absorbance values fitted using BindFit for the determination of the 1:1 association constant ($K_{1:1}$).

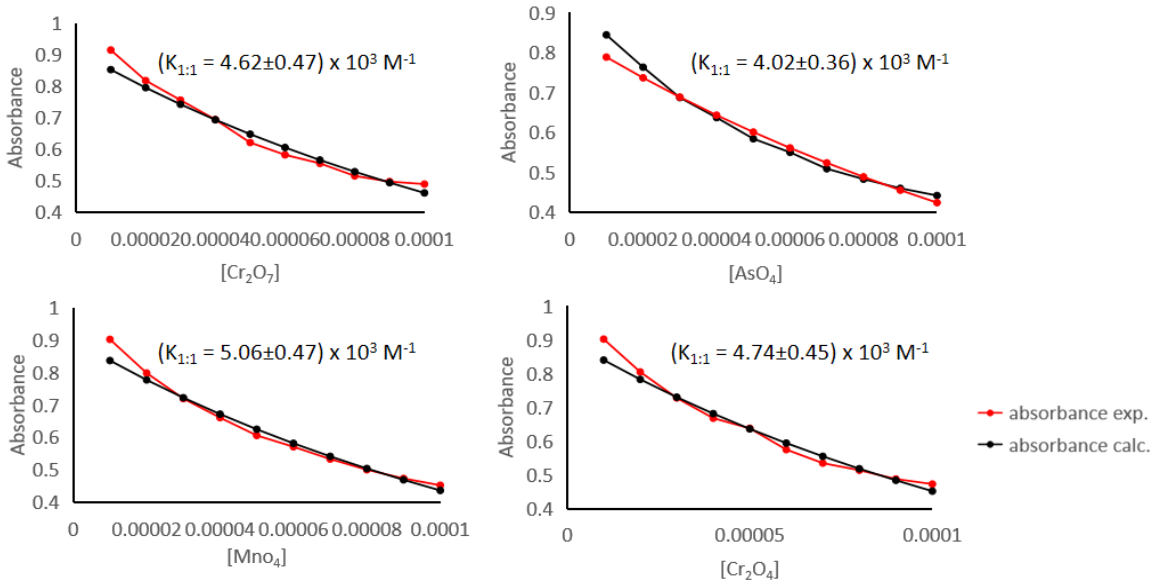

Figure 19. UV–Vis titration plots of **AT2** with $Cr_2O_7^{2-}$, AsO_4^{3-}, MnO_4^-, and CrO_4^{2-} showing experimental and calculated absorbance values fitted using BindFit for the determination of the 1:1 association constant ($K_{1:1}$).

Analysis of Association Constants (K_a)

The association constants ($K_{1:1}$) for receptors **AT1-AT3** toward the respective oxoanions were determined by the non-linear least-squares fitting of UV–Vis titration data using the BindFit platform, assuming a 1:1 host–guest binding model [58]. The calculated absorbance values closely matched the experimental data, as evidenced by the good overlap between experimental and calculated curves, confirming the validity of the proposed binding stoichiometry (**Figure 18-20**) [59].

In **Figure 18**, tripodal receptor **AT1**-anion complexes exhibited moderate binding affinities toward the investigated oxoanions. Among the anions tested, **AT1** showed the strongest interaction with AsO_4^{3-}, with a $K_{1:1}$ value of approximately 1.14×10^4 M^{-1}, followed by CrO_4^{2-} with 8.55×10^2 M^{-1}, $Cr_2O_7^{2-}$ with 4.05×10^3 M^{-1}, and MnO_4^- with 2.88×10^3 M^{-1}.

The relatively higher affinity toward AsO_4^{3-} can be attributed to its tetrahedral geometry and multiple oxygen atoms, which enable effective HB interactions with the thiourea –NH donors. In contrast, the absence of electron-withdrawing substituents in **AT1** limits the acidity of the thiourea –NH protons, resulting in comparatively weaker receptor-anion interactions.

AT2 (**Figure 19**) showed a noticeable enhancement in the binding strength of all the anions studied. The $K_{1:1}$ for **AT2** ranged from 4.02 - 5.06 × 10^3 M^{-1}, indicating consistently stronger interactions than those observed for **AT1**. The strongest binding was observed for MnO_4^- (5.06×10^3 M^{-1}) and $Cr_2O_7^{2-}$ (4.62×10^3 M^{-1}). The strong electron-withdrawing –NO_2 group increases the acidity of the thiourea NH protons, thereby strengthening the HB donation to the oxoanion oxygen atoms. This substituent effect enhances electrostatic stabilization of the receptor-anion complex and improves binding efficiency. The relatively uniform $K_{1:1}$ values across different anions also suggest that **AT2** had greater binding robustness compared to **AT1**.

In comparison, **AT3**, which incorporated a -CN substituent, demonstrated the highest binding affinities among the three receptors (**Figure 20**). This receptor exhibited a significantly enhanced association constant toward $C_2O_4^{2-}$, with a $K_{1:1}$ value of 1.88×10^4 M^{-1}, an order of magnitude higher than those observed for **AT1** and **AT2**. The $K_{1:1}$ for other anions, including MnO_4^- (4.96×10^3 M^{-1}) and $Cr_2O_7^{2-}$ (3.74×10^3 M^{-1}), further confirmed the superior binding performance of **AT3**. The electron-withdrawing nature of the –CN group substantially increases thiourea –NH acidity, leading to a more effective inductive electron-withdrawing effect, and thus a stronger and more directional N–H·O hydrogen bond. In contrast, the –NO_2 group may participate in intramolecular HB with adjacent N–H donors, reducing their availability for effective anion binding. Furthermore, the smaller and more linear nature of the –CN substituent allows better preorganization of the tripodal binding cavity, facilitating cooperative multidentate HB [60]. These combined effects resulted in the greater stabilization of the anion–receptor complex for **AT3**, leading to a higher $K_{1:1}$ relative to **AT2**. Additionally, the planar nature and charge density of CrO_4^{2-} may favour optimal geometric complementarity with the **AT3** binding cavity, resulting in enhanced complex stability.

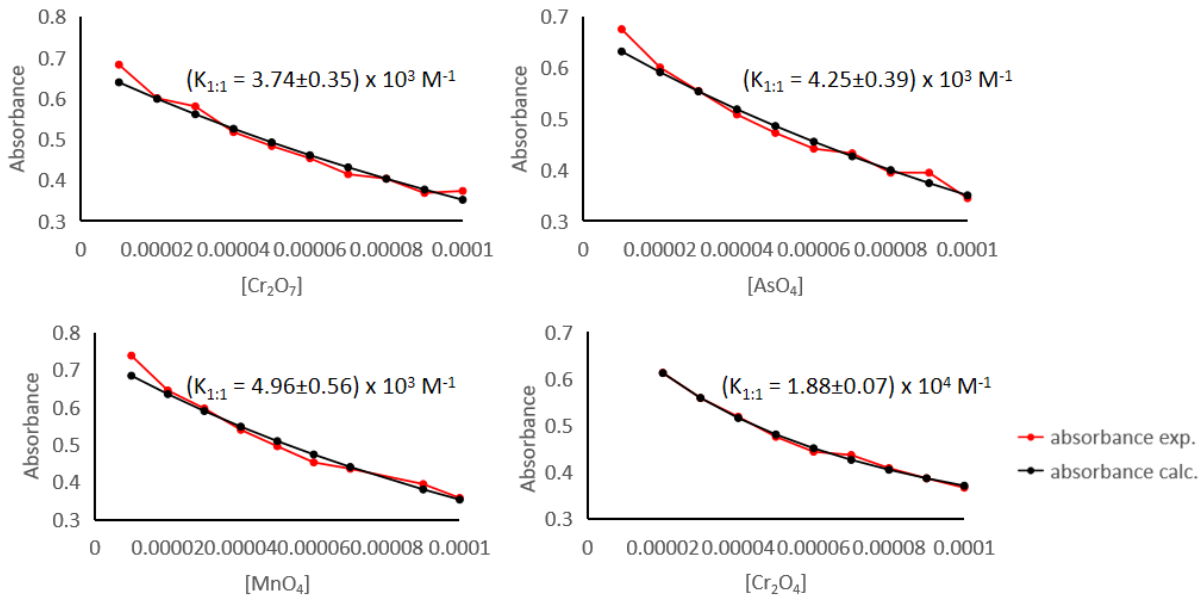

Figure 20. UV–Vis titration plots of **AT3** with $Cr_2O_7^{2-}$, AsO_4^{3-}, MnO_4^-, and CrO_4^{2-} showing experimental and calculated absorbance values fitted using BindFit for the determination of the 1:1 association constant ($K_{1:1}$).

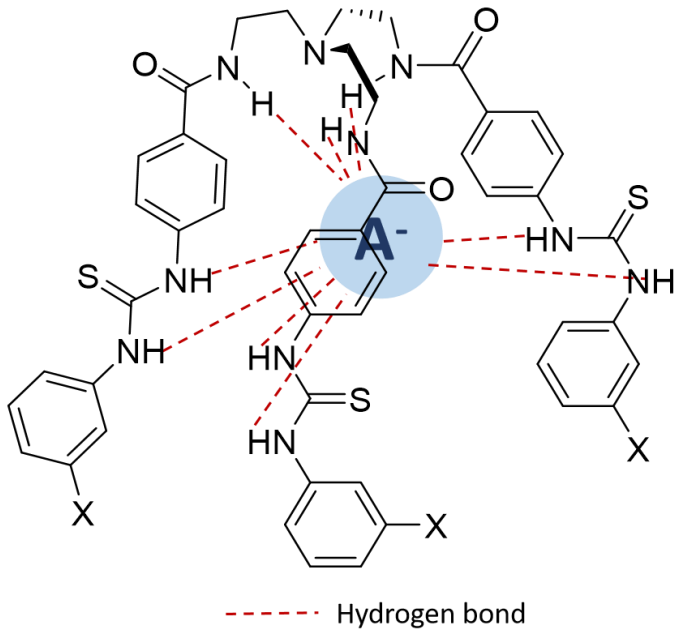

Figure 21. Anion encapsulation by the receptor is facilitated through NH···O hydrogen bonds.

The binding affinities of the receptor-anions followed the trend: **AT3** > **AT2** > **AT1**, indicating that receptor–anion interactions are governed not solely by substituent electron-withdrawing strength but by a balance between NH acidity, receptor preorganization, and secondary stabilizing interactions such as anion–π and ion–dipole forces. While the –NO_2 group is a stronger electron-withdrawing substituent, the –CN group provides sufficient NH acidification while preserving favourable receptor geometry and π-surface accessibility, enabling more effective convergent NH·O hydrogen bonding and additional non-covalent stabilization. The enhanced binding observed for **AT** can be rationalized by the proposed binding mode shown in **Figure 21,** where anion complexation occurs through multiple convergent NH O hydrogen bonds from amide and thiourea groups, complemented by ion-dipole and anion-π interactions. Experimental

absorbance values agreed well with BindFit calculations, supporting the 1:1 binding model and the reliability of extracted association constants. Although distinct isosbestic points were absent, Job plot analyses showed maxima at ~0.5 mole fraction, confirming predominant 1:1 stoichiometry [61]. Nonlinear fitting further indicated well-behaved binding equilibria. Overall, Job plot analysis and K_a values provided quantitative evidence of complex formation, with UV–Vis changes offering qualitative confirmation. The pseudo-isosbestic behaviour aligns with that of other flexible thiourea- and urea-based receptors, reflecting a gradual spectral evolution rather than an ideal two-state transition [17][58].

CONCLUSION

Three tripodal amide–thiourea receptors (**AT1-AT3**) were successfully synthesized and evaluated for tetrahedral oxoanion recognition. Spectroscopic analyses confirmed that anion binding occurred primarily through N–H·O hydrogen bonding interactions within a preorganized tripodal framework. UV–Vis titration results revealed consistent bathochromic and hypochromic responses, while Job plot and binding constant analyses supported a predominant 1:1 binding mode.

The binding affinities followed the trend **AT3** > **AT2** > **AT1**, demonstrating that substituent effects played a crucial role in modulating receptor performance. The –CN group in **AT3** provided an optimal balance between electron-withdrawing ability and structural preorganization, resulting in enhanced binding strength. In contrast, the $–NO_2$ group in **AT2**, although strongly electron-withdrawing, may lead to a reduced binding efficiency due to intramolecular interactions.

Overall, this work highlights the critical role of substituent effects in governing HB capability, electronic modulation, and anion recognition performance in tripodal amide–thiourea systems. The results establish the **AT3** framework as a promising scaffold for the selective optical sensing of environmentally relevant oxoanions. Furthermore, the identified structure–property relationships provide valuable guidance for the rational design of advanced supramolecular receptors for environmental monitoring and water quality assessment.

ACKNOWLEDGEMENTS

The authors would like to thank the Malaysian Ministry of Higher Education for financially supporting this research through the Fundamental Research Grant Scheme FRGS/1/2023/STG05/UIAM/02/1. The authors also acknowledge Kulliyyah of Science, International Islamic University Malaysia, for providing the research facilities.

REFERENCES

1. Arman, N. Z., Salmiati, S., Aris, A., Salim, M. R., Nazifa, T. H., Muhamad, M. S. and Marpongahtun, M. (2021) A review on emerging pollutants in the water environment: Existences, health effects and treatment processes. *Water*, **13**(**22**), 3258.

2. Hardyanti, N., Zaman, B., Putri, N. F., Phitaloka, A. B. D., Wahyuarta, M. B. and Purwono, P. (2025) Advanced ultrasound-assisted degradation of pharmaceutical wastewater: a sustainable solution for eutrophication control. *IOP Conference Series: Earth and Environmental Science*, **1556**(**1**), 012028.

3. Ahmed, S. A., Pinjari, N. S., Swami, M. V., Nilkanthe, P. P., and Palimkar, M. D. (2025) Health Effects and Remediation Measures for Nitrate Contamination in Water Resources. *Journal of Pharma Insights and Research*, **3**(**2**), 329–336.

4. Georgaki, M. N., Charalambous, M., Kazakis, N., Talias, M. A., Georgakis, C., Papamitsou, T. and Mytiglaki, C. (2023) Chromium in water and carcinogenic human health risk. *Environments*, **10**(**2**), 33.

5. Dugan, H. A., Skaff, N. K., Doubek, J. P., Bartlett, S. L., Burke, S. M., Krivak-Tetley, F. E. and Weathers, K. C. (2020) Lakes at risk of chloride contamination. *Environmental Science & Technology*, **54**(**11**), 6639–6650.

6. Eteiwi, S. M., Al-Eyadah, A. A., Al-Sarihin, K. K., Al-Omari, A. A., Al-Asaad, R. A. and Haddad, F. H. (2015) Potassium permanganate poisoning: A nonfatal outcome. *Oman Medical Journal*, **30**(**4**), 291.

7. Yeo, K. F. H., Li, C., Zhang, H., Chen, J., Wang, W. and Dong, Y. (2021) Arsenic removal from contaminated water using natural adsorbents: a review. *Coatings*, **11**(**11**), 1407.

8. Macreadie, L. K., Gilchrist, A. M., McNaughton, D. A., Ryder, W. G., Fares, M. and Gale, P. A. (2022) Progress in anion receptor chemistry. *Chem.*, **8**(**1**), 46–118.

9. Goodall, B. L., Ferguson, J. P. and Pye, C. C. (2024) Ab Initio Investigation of the Hydration of the Tetrahedral d0 Transition Metal Oxoanions NbO_4^{3-}, TaO_4^{3-}, CrO_4^{2-}, MoO_4^{2-}, WO_4^{2-}, MnO_4^{-}, TcO_4^{-}, ReO_4^{-}, and of FeO_4, RuO_4, and OsO_4. *Liquids*, **4**(**3**), 539–580.

10. Semysim, F. A., Ridha, R. K., Azooz, E. A. and Snigur, D. (2024) Switchable hydrophilicity solvent-assisted solidified floating organic drop microextraction for separation and determination

of arsenic in water and fish samples. *Talanta*, **272**, 125782.

11. Muslim, N. M., Abbood, F. K., Hammood, N. H. and Azooz, E. A. (2024) Air-assisted solidified floating organic drop microextraction method based on green supramolecular solvent for arsenic and selenium qantification in water and food samples. *Journal of Food Composition and Analysis*, **134**, 106558.

12. Azooz, E. A., Moslim, J. R. and Jawad, S. K. (2020) Cloud Point Extraction Methodology for Separation, Extraction and Preconcentration of Mn (VII) Coupled with Spectroscopy for Determination in Different Samples. *Biochemical & Cellular Archives*, **20**(**1**), 2641–2648.

13. Murfin, L. C., Chiang, K., Williams, G. T., Lyall, C. L., Jenkins, A. T. A., Wenk, J. and Lewis, S. E. (2020) A colorimetric chemosensor based on a Nozoe azulene that detects fluoride in aqueous/ alcoholic media. *Frontiers in Chemistry*, **8**, 10.

14. Yang, L., Liu, Y. L., Liu, C. G., Fu, Y. and Ye, F. (2021) A naked-eye visible colorimetric and ratiometric chemosensor based on Schiff base for fluoride anion detection. *Journal of Molecular Structure*, **1236**, 130343.

15. McNaughton, D. A., Ryder, W. G., Gilchrist, A. M., Wang, P., Fares, M., Wu, X. and Gale, P. A. (2023) New insights and discoveries in anion receptor chemistry. *Chem.*, **9**(**11**), 3045–3112.

16. Jia, C., Zuo, W., Zhang, D., Yang, X. J. and Wu, B. (2016) Anion recognition by oligo-(thio) urea-based receptors. *Chemical Communications*, **52**(**62**), 9614–9627.

17. Manna, U., Portis, B., Egboluche, T. K., Nafis, M. and Hossain, M. A. (2021) Anion binding studies of urea and thiourea functionalized molecular clefts. *Frontiers in Chemistry*, **8**, 575701.

18. Kundu, S., Egboluche, T. K. and Hossain, M. A. (2023) Urea-and thiourea-based receptors for anion binding. *Accounts of Chemical Research*, **56**(**11**), 1320–1329.

19. Gomez-Vega, J., Vasquez-Cornejo, A., Juárez-Sánchez, O., Corona-Martínez, D. O., Ochoa-Terán, A., López-Gastelum, K. A. and Lara, K. O. (2024) Thiourea-based receptors for anion recognition and signaling. *ACS Omega*, **9**(**4**), 4412–4422.

20. Dey, S. K., Basu, A., Chutia, R. and Das, G. (2016) Anion coordinated capsules and pseudocapsules of tripodal amide, urea and thiourea scaffolds. *RSC Advances*, **6**(**32**), 26568–26589.

21. Mohammed, F. A., Xiao, T., Wang, L. and Elmes, R. B. (2024) Macrocyclic receptors for anion recognition. *Chemical Communications*, **60**(**83**), 11812–11836.

22. Ghosh, I., Pramanik, S., Islam, A. S., Dutta, A. and Ghosh, P. (2026) A Benzothiadiazole-Based Thiourea Receptor for Selective Chloride Extraction and Reversible Fluoride Sensing. *Chemistry–An Asian Journal*, **21**(**1**), e70183.

23. Rajendran, N., Kamaraj, K., Janakiraman, S., Saral, M., Dixneuf, P. H. and Bheeter, C. B. (2023) A sustainable metal and base-free direct amidation of esters using water as a green solvent. *RSC advances*, **13**(**22**), 14958–14962.

24. Alsawat, M., Adam, A. M. A., Refat, M. S., Alsuhaibani, A. M. and El-Sayed, M. Y. (2024) Structural, spectroscopic, and morphological characteriza-tions of metal-based complexes derived from the reaction of 1-phenyl-2-thiourea with Sr^{2+}, Ba^{2+}, Cr^{3+}, and Fe^{3+} ions. *Bulletin of the Chemical Society of Ethiopia*, **38**(**6**), 1803–1814.

25. Rahman, F. U., Bibi, M., Khan, E., Shah, A. B., Muhammad, M., Tahir, M. N. and Batiha, G. E. S. (2021) Thiourea derivatives, simple in structure but efficient enzyme inhibitors and mercury sensors. *Molecules*, **26**(**15**), 4506.

26. Hussain, Z., Mahmood, A., Shah, Q., Imran, A., Mughal, E. U., Khan, W. and Mumtaz, A. (2022) Synthesis and evaluation of amide and thiourea derivatives as carbonic anhydrase (CA) inhibitors. *ACS Omega*, **7**(**50**), 47251–47264.

27. Nasri, N. A. M. and Jumal, J. (2020) A Preliminary Study on Detection of Cadmium (II) Ion Using Benzoyl Phenylthiourea. *Journal of Wastes and Biomass Management (JWBM)*, **2**(**1**), 09–14.

28. Hansen, P. E., Vakili, M., Kamounah, F. S. and Spanget-Larsen, J. (2021) NH stretching frequencies of intramolecularly hydrogen-bonded systems: an experimental and theoretical study. *Molecules*, **26**(**24**), 7651.

29. Wieczorkiewicz, P. A., Szatylowicz, H. and Krygowski, T. M. (2022) Energetic and Geometric Characteristics of Substituents, Part 3: The Case of NO_2 and NH_2 Groups in Their Mono-Substituted Derivatives of Six-Membered Heterocycles. *Symmetry*, **14**(**1**), 145.

30. Smith, B. (2019) Organic nitrogen compounds IV: nitriles. *Spectroscopy*, **34**(**7**), 18–21.

31. Choi, S., Park, J., Kwak, K. and Cho, M. (2021) Substituent Effects on the Vibrational Properties of the CN Stretch Mode of Aromatic Nitriles: IR

Probes Useful for Time-resolved IR Spectroscopy. *Chemistry–An Asian Journal*, **16**(**18**), 2626–2632.

32. Naeem, H. S., Jaber, I., Sapari, S., Razak, N. H. A., and Ilyana, F. (2024) Microwave vs. Reflux Synthesis of Bis-Thiourea Derivative: Yield Optimization, Crystallographic Understanding and Optical Sensing Potential. *Sains Malaysiana*, **53**(**8**), 1937–1952.

33. Essid, M. and Mughal, E. U. (2025) Push–pull heterocycles and beyond: recent developments in absorption, emission, and ICT properties. *RSC Advances*, **15**(**45**), 37609–37644.

34. Rančić, M. P., Stojiljković, I., Milošević, M., Prlainović, N., Jovanović, M., Milčić, M. K. and Marinković, A. D. (2019) Solvent and substituent effect on intramolecular charge transfer in 5-arylidene-3-substituted-2, 4-thiazolidinediones: Experimental and theoretical study. *Arabian Journal of Chemistry*, **12**(**8**), 5142–5161.

35. Sapari, S., Zakariah, E. I., Razak, N. H. A., Ramzan, I., Numin, M. S., Lee Yook Heng and Hasbullah, S. A. (2021) A comparative study of microwave-assisted and conventional heating methods of the synthesis of 1-(naphthalene-1-yl)-3-(o, m, p-tolyl) thioureas, dft analysis, antibacterial evaluation and drug-likeness assessment. *Sains Malaysiana*, **50**(**3**), 743–751.

36. Gunawan, R. and Nandiyanto, A. (2021) How to read and interpret 1H-NMR and 13C-NMR spectrums. *Indonesian Journal of Science and Technology*, **6**(**2**), 267–298.

37. Mohnish, M., Ramavath, V., Ghule, V. D. and Sarangapani, R. (2025) Computation of 1H NMR chemical shifts: structural assessment of energetic materials. *Journal of Molecular Modeling*, **31**(**9**), 230.

38. Baranac-Stojanović, M. (2018) Can variations of 1H NMR chemical shifts in benzene substituted with an electron-accepting (NO_2)/donating (NH_2) group be explained in terms of resonance effects of substituents? *Chemistry–An Asian Journal*, **13**(**7**), 877–881.

39. Zhao, Y., Li, T., Kjaerulff, L., Venter, H., Coriani, S., Møller, B. L. and Staerk, D. (2023) Orthogonal Reversed-Phase C18 and Pentafluorophenyl HPLC Separation for Phytochemical Profiling of Serrulatanes in Eremophila denticulata. *Journal of Natural Products*, **86**(**12**), 2638–2650.

40. Dahlqvist, E., Morais, E. M. and Martinelli, A. (2024) Synthesis and characterization of new imidazolium based protic ionic liquids obtained by nitro-and cyano-functionalization. *Journal of Molecular Liquids*, **415**, 126269.

41. Zavala-Contreras, B., Santacruz-Ortega, H., Orozco-Valencia, A. U., Inoue, M., Ochoa Lara, K. and Navarro, R. E. (2021) Optical anion receptors with urea/thiourea subunits on a tentagel support. *ACS Omega*, **6**(**14**), 9381–9390.

42. Matsumoto, S., Takamori, M. and Akazome, M. (2023) Bathochromic shift of fluorescence peak in dipyrrolo [1, 2-a: 2′, 1′-c] quinoxaline by introducing each of electron-donating and electron-withdrawing substituent. *Molecules*, **28**(**7**), 2896.

43. Manna, U., Portis, B., Egboluche, T. K., Nafis, M. and Hossain, M. A. (2021) Anion binding studies of urea and thiourea functionalized molecular clefts. *Frontiers in Chemistry*, **8**, 575701.

44. Kumar, J., Kumar, N. and Hota, P. K. (2020) Optical properties of 3-substituted indoles. *RSC Advances*, **10**(**47**), 28213–28224.

45. Orenha, R. P., da Silva, V. B., Caramori, G. F., Piotrowski, M. J., Nagurniak, G. R. and Parreira, R. L. T. (2021) The design of anion–π interactions and hydrogen bonds for the recognition of chloride, bromide and nitrate anions. *Physical Chemistry Chemical Physics*, **23**(**19**), 11455–11465.

46. Kundu, S., Egboluche, T. K., Yousuf, Z. and Hossain, M. A. (2021) Spectroscopic and colorimetric studies for anions with a new urea-based molecular cleft. *Chemosensors*, **9**(**10**), 287.

47. Kaspar, F. (2023) Quality data from messy spectra: How isometric points increase information content in highly overlapping spectra. *ChemBioChem*, **24**(**7**), e202200744.

48. Hassan, E., Vinodh, M., Alipour, F. H. and Al-Azemi, T. F. (2025) Bis-urea anion receptors: influence of receptor structure and anion nature on binding affinity and stability. *RSC advances*, **15**(**33**), 26623–26631.

49. Bagha, H., Hein, R., Lim, J. Y., Durr, C. B., Sambrook, M. R. and Beer, P. D. (2024) Halogen Bonding Tripodal Metallo-Receptors for Phosphate Recognition and Sensing in Aqueous-Containing Organic Media. *Chemistry–A European Journal*, **30**(**2**), e202302775.

50. Maslowska-Jarzyna, K., Korczak, M. L., Wagner, J. A. and Chmielewski, M. J. (2021) Carbazole-based colorimetric anion sensors. *Molecules*, **26**(**11**), 3205.

51. Namashivaya, S. S., Oshchepkov, A. S., Ding, H., Förster, S., Khrustalev, V. N. and Kataev, E. A. (2019) Anthracene-based receptors with a turn-on fluorescence response for nitrate. *Organic Letters*, **21**(**21**), 8746–8750.

52. Emami Khansari, M., Hasan, M. H., Johnson, C. R., Williams, N. A., Wong, B. M., Powell, D. R. and Hossain, M. A. (2017) Anion complexation studies of 3-nitrophenyl-substituted tripodal thiourea receptor: a naked-eye detection of sulfate via fluoride displacement assay. *ACS Omega*, **2**(**12**), 9057–9066.

53. Picci, G., Montis, R., Gilchrist, A. M., Gale, P. A. and Caltagirone, C. (2024) Fluorescent and colorimetric sensors for anions: Highlights from 2020 to 2022. *Coordination Chemistry Reviews*, **501**, 215561.

54. Manna, U., Das, G. and Hossain, M. A. (2022) Insights into the binding aspects of fluoride with neutral synthetic receptors. *Coordination Chemistry Reviews*, **455**, 214357.

55. Sun, J., Decato, D. A., Bryantsev, V. S., John, E. A. and Berryman, O. B. (2023) The interplay between hydrogen and halogen bonding: substituent effects and their role in the hydrogen bond enhanced halogen bond. *Chemical Science*, **14**(**33**), 8924–8935.

56. Nayak, B., Halder, S., De, S. and Das, G. (2019) Binding consistency of anions by the effect of aromatic meta-substitution of bis-urea receptors: entrapment of hexafluorosilicate clusters. *CrystEngComm*, **21**(**46**), 7172–7181.

57. Bhat, M. P., Vinayak, S., Yu, J., Jung, H. Y. and Kurkuri, M. (2020) Colorimetric receptors for the detection of biologically important anions and their application in designing molecular logic gate. *ChemistrySelect*, **5**(**42**), 13135–13143.

58. Gomez-Vega, J., Soto-Cruz, J. M., Juarez-Sanchez, O., Santacruz-Ortega, H., Gálvez-Ruiz, J. C., Corona-Martínez, D. O. and Ochoa Lara, K. (2022) Tritopic bis-urea receptors for anion and ion-pair recognition. *ACS Omega*, **7**(**26**), 22244–22255.

59. Kubik, S. (2024) Supramolecular chemistry: from concepts to applications. *Walter de Gruyter GmbH & Co KG*.

60. Suponitsky, K. Y. and Strizhenko, K. V. (2022) Synthesis and Crystal Structure of 3-(4-Cyano-3-nitro-1 H-pyrazol-5-yl)-4-nitrofurazan: Comparison of the Influence of the NO2 and CN Groups on Crystal Packing and Density. *Molbank*, **2023**(**1**), M1533.

61. Singh, G., Priyanka, Sushma, Pawan, Mohit, Satija, P. and Espinosa-Ruíz, C. (2021) Synthesis and Characterization of Antioxidant Biphenyl Appended 1, 2, 3-Triazoles as Potential Chemo-Sensor for Sn^{2+} Ions: Excellent Selectivity and Low Detection Limit. *ChemistrySelect*, **6**(**30**), 7613–7621.